

Boosting the efficiency up to 33 % for chalcogenide tin mono-sulfide-based heterojunction solar cell using SCAPS simulation technique

Amarjeet Kumar^a, Rahutosh Ranjan^a, Vijay Kumar Mishra^b, Neelabh Srivastava^a, Rajanish N. Tiwari^c, Laxman Singh^{d,*}, Arvind Kumar Sharma^{a, **}

^a Department of Physics, School of Physical Sciences, Mahatma Gandhi Central University, Motihari, 845401, Bihar, India

^b Department of Physics, Institute of Applied Sciences & Humanities, GLA University, Mathura, 281406, UP, India

^c Department of Chemistry, School of Physical Sciences, Mahatma Gandhi Central University, Motihari, 845401, Bihar, India

^d Department of Chemistry, Siddhartha University, Kapilavastu, Siddharth Nagar, 272202, India

ARTICLE INFO

Keywords:

Chalcogenide tin-mono sulfide
Heterojunction photovoltaic cell
Active hole transport layer
Electron transport layer
SCAPS-1D
Solar cell capacitance simulator in 1D
Carrier recombination

ABSTRACT

In the present article, an FTO/n-ZnO/SnS/Sb₂S₃/Au heterojunction photovoltaic cell structure was modeled and the cell performance in terms of output parameters viz. open circuit voltage (V_{oc}), short-circuit current density (J_{sc}), efficiency (η) and fill factor (FF) by varying carrier concentration, and thickness of different layers involved, was studied at ambient conditions. The overall theoretical performance of the designed photovoltaic cell was examined using SCAPS 1-D simulation programme. The simulation programme operates by resolving semiconductor equations such as the Poisson equation, drift-diffusion equation, and continuity equation for both electrons and holes. The equations are generally solved in one-dimension (1D) in a steady state condition. The role of Sb₂S₃ HTL on the performance study of tin sulfide chalcogenide-based heterojunction photovoltaic cell (HPVC) was also analyzed. Moreover, the impact of functioning temperature between 273 K and 350 K on the performance of photovoltaic cell was observed, and an increase in temperature resulted in poor performance. The impact of different metal back contact work functions and some more electrical parameters viz. series-shunt resistances, defect concentration of layers and interfaces, and radiative recombination coefficients were also observed on HPVC. The simulation results revealed that the HTL Sb₂S₃ forms proper band alignment with the SnS chalcogenide absorber layer and enhanced the efficiency, η of HPVC by lessening the carrier recombination at the rear contact side. The dislocation and interface defect reduced significantly which leads to the smooth conduction of hole carriers, therefore, preventing of minority carriers to recombine within the absorber. A significant increase in the efficiency ~33.24 % together with performance cell parameters J_{sc} ~34.38 mA/cm², V_{oc} ~1.09 V, and FF ~88.49 % was observed.

1. Introduction

In recent years, thin film-based photovoltaic devices have received remarkable attention worldwide for their low cost, stability, highly efficient, and mass production. However, the commercial development and production still have further challenges like toxicity, earth abundance of material components, and heavy metals like lead which are major concerns from environmental perspective. In such a challenging condition, the thin film photovoltaic cells have shown its likely to meet our requirements for largescale production. The technology of thin film also invites for the opportunity to go beyond the conventional limit of

silicon technology and to reach an economical goal with earth-abundant, inexpensive, and nontoxic materials. Therefore, thin film has been fascinated as a preference to the scientific community. It is observed that, suitable electrical and optical characteristics, such as good optical absorption coefficient, proper band gap, and good quantum yield of constituent materials of thin films lead to accomplish the desired transformation into efficiency. The advancement of photovoltaic cell applications using different kinds of materials has resulted in a substantial rise in power conversion efficiency. However, the toxicity and its abundances limit its applications towards its commercialization at large scale.

* Corresponding author.

** Corresponding author.

E-mail addresses: laxmanresearcher@suksn.edu.in (L. Singh), arvindkumar@mgcub.ac.in (A.K. Sharma).

Table 1Simulation parameters for defects at $\text{Sb}_2\text{S}_3/\text{SnS}$ and $\text{SnS}/\text{n-ZnO}$.

Parameters (unit)	$\text{Sb}_2\text{S}_3/\text{SnS}$	$\text{SnS}/\text{n-ZnO}$
Defect type	Neutral	Neutral
Capture cross section electrons (cm^2)	1×10^{-19}	1×10^{-19}
Capture cross section holes (cm^2)	1×10^{-19}	1×10^{-19}
Reference for defect energy level E_t	Above the highest	Above the highest
Energy with respect to Reference (eV)	E_v	E_v
Total density (integrated over all energies) (cm^{-2})	1.00×10^{11}	1.00×10^{11}

In order to choose an appropriate material for the absorber layer in $p-n$ heterojunction, the absorber layer should have the properties to absorb solar radiation light much feasible so as to stimulate charge carriers e^- from lower energy to higher energy levels and the have ability to pass the generated excited e^- 's from the photovoltaic cell heterojunction to the external circuit. On the other hand, if a very high absorbent material is utilized for the absorber layer, then there could be a possibility of absorption of photon very near to the surface which lowers the efficiency. Generally, we take a broad band gap window layer material to avoid the surface recombination at the forward-side. Nevertheless, the carrier regulation of front-side surface and absorber characteristics is hard to accomplish and face a substantial loss. Thereby, a proper accent is put on the rear metal contact face in heterojunction to improve and adjust the photo-conversion efficiency (PCE) from its typical range.

Photovoltaic cells based on IV-VI chalcogenides semiconducting compounds materials are amid the foremost contenders for inexpensive photovoltaic conversion of energy from the sun owing to their very large value of absorption coefficients and consequently the less material utilization for their manufacture. The contender chalcogenide tin mono-sulfide (SnS) of the orthorhombic structure has accomplished some attention, at present time it is consumed as an ideal absorber in the development of thin-film solar cell technology [1–4]. In the advancement of photovoltaic devices, chalcogenide tin mono-sulfide has various merits, such as better absorption coefficient order of 10^7 m^{-1} and its appropriate bandgap close to $\sim 1.30 \text{ eV}$ [5,6], which leads SnS to absorb the sun radiation spectrum above the band gap in less than $1 \mu\text{m}$ thick. SnS is an economical photovoltaic cell material that is non-toxic, earth-abundant and it can be manufactured over an easy non-vacuum and vacuum-based routes viz. spray-pyrolysis [7], spin-coating [8], dip-coating [9], sputtering [10], thermal-evaporation [11], chemical vapor deposition [12], etc. The thin film from SnS is safeguards against

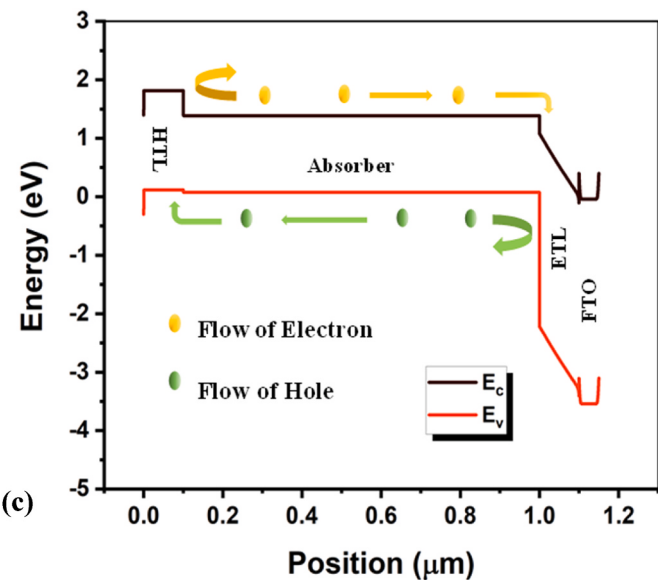


Fig. 1b. (c)An illustration of energy band diagram based on different electrical parameters for modeled heterojunction photovoltaic cell.

flaws and impurities, thereby providing an effective and financially viable replacement for silicon solar cells [13,14]. However, the performance of SnS-based solar cells remains limited due to typical bulk defect density and interface losses caused by conduction-band offset, which results in interfacial recombination [13,15]. Currently, various SnS-based heterojunction solar cells are being designed, such as ITO/SnS, ZnS/SnS, CdS/SnS, and TiO_2/SnS [16–18] have been reported. Xu et al. statistically examined the several heterojunction structures of chalcogenide tin mono-sulfide-based photovoltaic cells (ZnS/SnS, ZnO/SnS, CdO/SnS, a-Si/SnS, and SnS/c-Si) to obtain optimum efficiency, the ZnS/SnS heterostructure had recorded the greatest efficiency of 16.26 % [18]. The maximum anticipated experimental efficiency of a thin film solar cell based on SnS is 4.63 % [3]. Numerical investigation was conducted on the heterojunctions of CdS/SnS, ZnS/SnS, ZnO/SnS, a-Si/SnS, and SnS/c-Si, employing numerical analysis techniques. Based on the simulated data, the ZnS/SnS heterojunction exhibits a maximum conversion efficiency of 16.26 % [18]. Lin et al. optimized the thickness of the SnS and the n-type GaN layer to create GaN/SnS solar cells with a

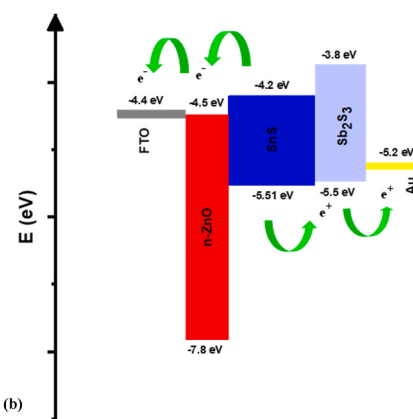
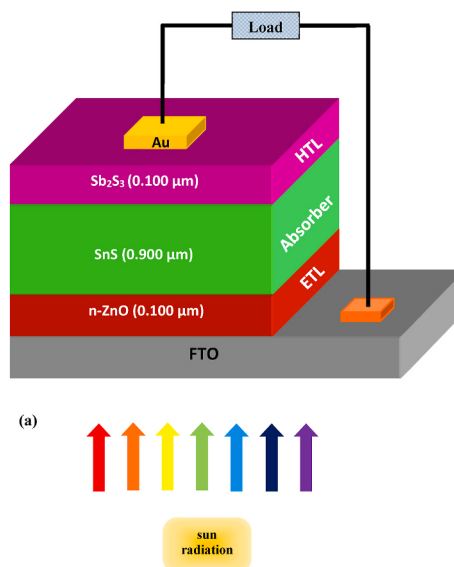


Fig. 1a. Illustration of (a) A schematic Energy band diagram (b) Energy band alignment diagram for modeled heterojunction photovoltaic cell.

Table 2

Material Parameters used in simulation [62–67].

Material Parameters	FTO	n-ZnO (ETL)	SnS (Abs.)	Sb ₂ S ₃ (HTL))
Thickness (μm)	0.050	0.100	0.900	0.100
Band gap (eV)	3.5	3.3	1.31	1.7
Electron affinity (eV)	4.0	4.5	4.2	3.8
Dielectric permittivity	9.0	9.0	13.0	7.0
CB effective density of states (cm^{-3})	2.2×10^{18}	2.2×10^{18}	1.18×10^{18}	2.0×10^{19}
VB effective density of states (cm^{-3})	1.8×10^{19}	1.8×10^{19}	4.76×10^{18}	1.0×10^{19}
Electron thermal velocity (cm/s)	1.0×10^7	1.0×10^7	1.0×10^7	1.0×10^7
Hole thermal velocity (cm/s)	1.0×10^7	1.0×10^7	1.0×10^7	1.0×10^7
Electron mobility (cm^2/Vs)	20.0	100.0	130	7.0×10^{-2}
Hole mobility (cm^2/Vs)	10.0	25.0	4.3	2.0×10^{-2}
Shallow donor density N_D (cm^{-3})	2.0×10^{19}	1.0×10^{16}	0	0
Shallow acceptor density N_A (cm^{-3})	0	0		1×10^{21}
Defect density N_t (cm^{-3})	N/A	1×10^{14}	1×10^{14}	1×10^{14}
Charge type		Neutral	Neutral	Neutral

26.34 % efficiency [19]. Farshad et al. reported an optimized 28.92 % efficiency for the perovskite/SnS tandem device utilizing numerical modeling [20]. A novel optimized solar cell design (a-Si: H/SnS/ZnSe/ITO) achieves a significant efficiency gain of 26.91 % [15]. SILAR-fabricated SnS quantum dot solar cell reaches an optimal efficiency of 0.54 % with 311 mV open circuit voltage and 4.86 mA/cm² short circuit current density [21]. Shivani Gohri et al. achieved a 14.02 % efficiency for SnS-based solar cells utilizing the GLAD approach and the CZTSSe buffer layer [14]. Rajeshwari Garain et al., simulate a glass/ITO/ZnO/CdS/SnS/metal contact and get an efficiency of 8.77 %

[22]. The prepared FTO/ZnO/SnS heterojunction solar cell surpassed other structures having a conversion efficiency of 0.96 %, superior to FTO/CdS/SnS and FTO/SnS₂/SnS heterojunction [23]. Minbashi et al. developed a SnS thin film using the glancing angle deposition (GLAD) technique and reached the highest efficiency of 7.68 % for SnS₈₅ using SCAPS simulation [2]. Using SCAPS-1D simulation software, a new (ITO/CeO₂/SnS/NiO/Mo) heterostructure of the SnS-based solar cell with the highest PCE of 25.1 % was reported by S. Ahmed et al. [24]. It is crucial to comprehend the mechanism of device and performance of a SnS-based photovoltaic cell in order to improve the efficiency. An analysis of the photovoltaic cell's mechanism and behavior from a theoretical perspective supports us to better comprehend the device. In addition, theoretical analysis allows optimization of several specifications and understanding their impression on the photovoltaic cell, which is not feasible in experiments. thereby, theoretical investigation along with experimental investigations are significant to comprehend the device engineering and physics in deep. To achieve best photovoltaic performance of a chalcogenide SnS-based solar cell, structure is remodeled by introducing *p*⁺ layer sandwiched between the absorber and rear contact of electron, and using TCO as a rear contact [25]. Since the achievement of highly efficient SnS-based heterojunction solar cells is hindered by the open-circuit voltage, which serves as a significant limiting factor for solar cell applications. It has been observed that the open-circuit voltage measurement of numerous solar cell configurations falls short of the predicted outcome. Reduction to this value can occur as a result of the recombination of charge carriers within the junction. In order to improve the efficiency of SnS-based heterojunction solar cells, researchers have recommended the incorporation of a back surface field (BSF) layer or a hole transport layer (HTL) [22–25]. This is because the recombination loss of carriers at the back surface is a major contributing factor to the limited performance of these solar cells. By minimizing this loss, solar cell performances can significantly be enhanced. Regrettably, the insufficient carrier transportation and collection, along with the occurrence of interface recombination involving the reported BSFs or HTLs, persistently lead to a shortage in open-circuit voltage and short-circuit current. As a consequence, the overall efficiency of solar cells remains compromised. To ensure optimal performance and affordability, it is crucial to design a new heterojunction cell architecture for SnS-based which could be highly efficient and cost-effective. In

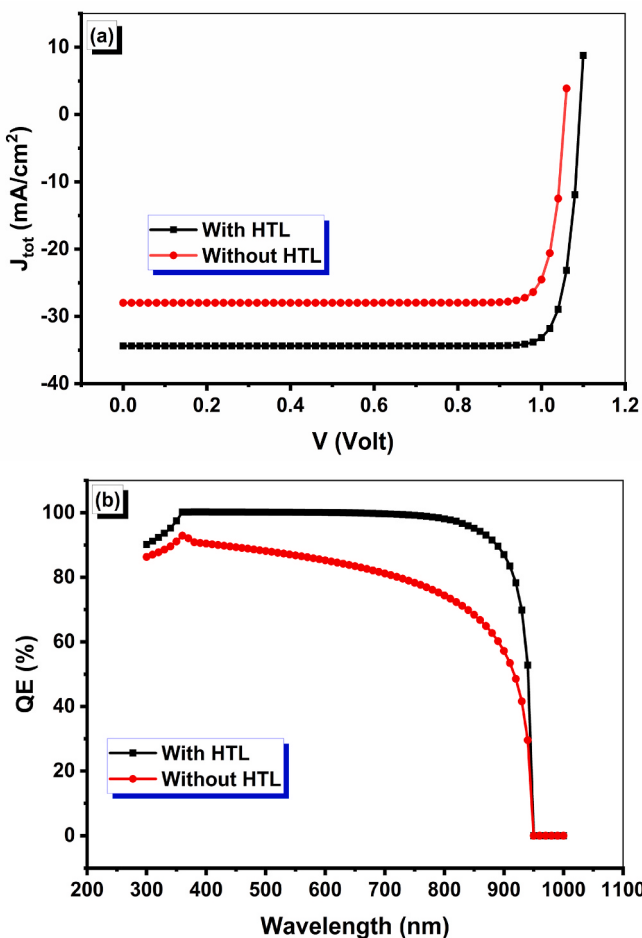


Fig. 2. (a) Simulated J-V characteristics and (b) Quantum efficiency as a function of wavelength of heterojunction photovoltaic cell with and without HTL.

Table 3Comparison on solar cell performance of SnS - based solar cell without and with HTL Sb₂S₃.

Structures	Voc(V)	J _{sc} (mA/cm ²)	FF (%)	η (%)
FTO/n-ZnO/SnS/Au (Without HTL)	1.05	27.99	88.44	26.15
FTO/n-ZnO/SnS/Sb ₂ S ₃ /Au (With HTL)	1.09	34.38	88.49	33.24

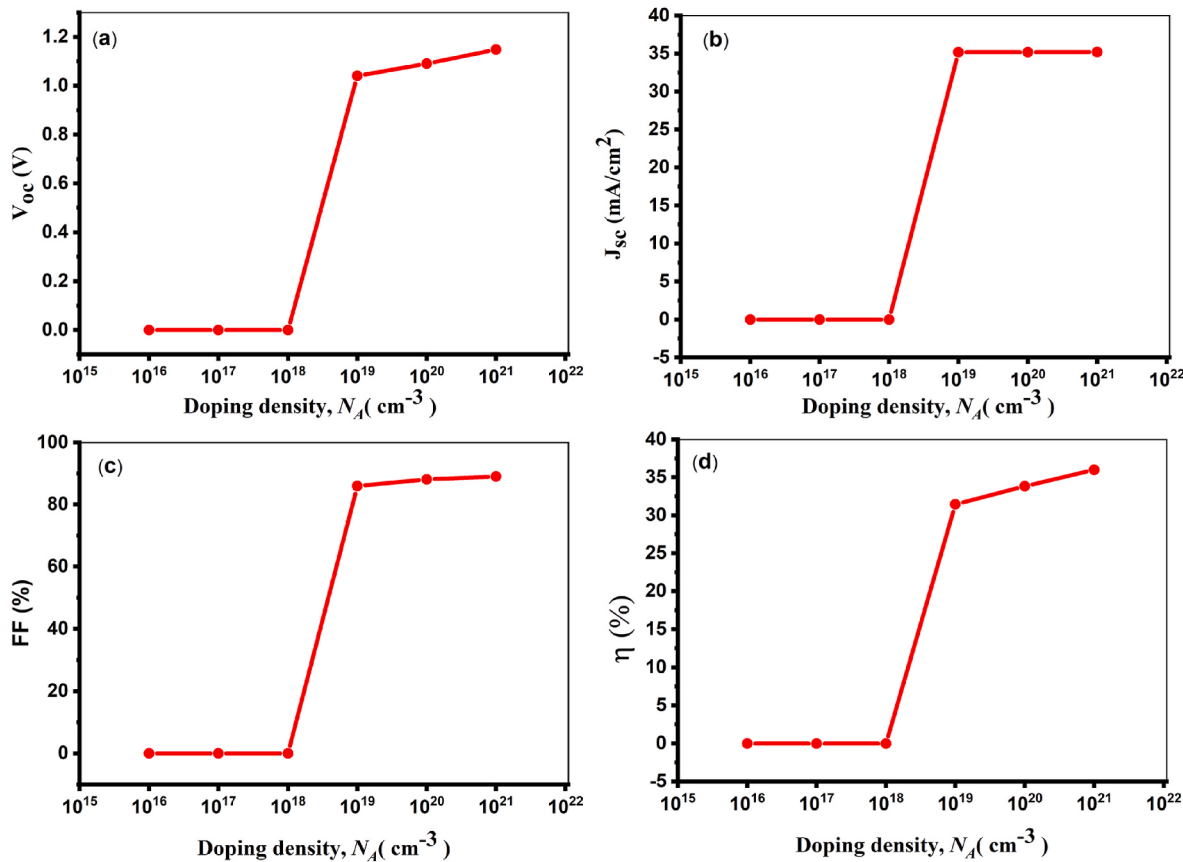


Fig. 3. (a–d): Effect of doping density of chalcogenide tin-mono sulfide absorber on output parameters such as V_{oc} , J_{sc} , FF, and η of a photovoltaic cell.

the most recent work, Hosen and Ahmed have observed through the simulation analysis that owing to recombination of charge carrier in junction, insufficient carrier transport and interface recombination with HTL, they have received poor photovoltaic performance of chalcogenide SnS-based photovoltaic cell [26]. A numerous HTLs have been analyzed by simulating the J-V characteristics with proper band alignment such as Cu_2O NiO_x , CuI [26], providing the efficiency of 8.22 %, 7.38 %, and 7.39 % respectively.

In this work, we have introduced Sb_2S_3 as p^+ type layer at the rear surface of a photovoltaic cell. The Sb_2S_3 semiconductors have high absorption coefficient, relative less toxic, and earth abundance. Sb_2S_3 serves as a V-VI semiconductor with good opto-electrical characteristics that is useful for a variety of opto-electronic devices due to its high absorption coefficient, variable bandgap $\approx 1.1\text{eV}$ – 1.7eV , inherent p-type conductivity, carrier mobility, low toxicity, and low melting point [27, 28]. So far, a maximum efficiency of 7.10 % has been observed for the planar superstrate Sb_2S_3 structural device [29]. The poor performance is mostly due to substantial surface-induced recombination losses caused by improper energy-level alignment and interface flaws [30]. A $\text{Mo}/\text{Sb}_2\text{S}_3/\text{CdS}/\text{i-ZnO}/\text{ZnO:Al}/\text{metal}$ contact heterojunction exhibiting the efficiency of 9.51 % is simulated [28]. Similarly, Xiao et al. found that $\text{FTO}/\text{ZnS}/\text{Sb}_2\text{S}_3/\text{Cu}_2\text{O}/\text{Au}$ had a numerical efficiency of 16.65 % [31]. Glass/FTO/ TiO_2 / Sb_2S_3 solar cells with HTLs V1236 and P3HT have attained efficiencies of 3.9 % and 3.7 %, respectively [27]. In addition to that, S. Barthwal et al. simulated a $\text{Zn}(\text{O}_{0.3}\text{S}_{0.7})/\text{Sb}_2\text{S}_3/\text{CuSCN}/\text{back contact}$ heterostructure to attain an efficiency of 13.88 % in normal n-i-p solar cells as well as 15.89 % in HTL-free Sb_2S_3 solar cells [30]. In another study, Sb_2S_3 is used as an HTL with CdTe as absorber layer and manifested PEC of 28.41 % [32]. In another study when Sb_2S_3 used as HTL ($\text{Ni}/\text{Sb}_2\text{S}_3/\text{CZTS}/\text{WS}_2/\text{FTO}/\text{Al}$) gained a photo conversion efficiency of 30.63 % [33]. In addition, the

Sb_2S_3 has effective band alignment with the chalcogenide tin mono-sulfide (SnS) absorber. The transport of hole carrier and deterrence of minority charge carriers from SnS leads an effortless transportation of photo generated holes from SnS absorber to rear contact with HTL [18, 28, 34, 35].

Numerous theoretical investigation and simulation are performed with ZnO/SnS heterostructure when ZnO used as a ETL, which resulted in efficiency of 12.08 % [36, 37]. In SCAPS-1D simulation the structure n-ZnO/SnS has achieved $V_{OC} \sim 0.24\text{V}$, $J_{sc} \sim 19.4\text{ mA/cm}^2$, FF $\sim 42.97\text{ \%}$, $\eta \sim 2.46\text{ \%}$. After studying and analyzing several published articles [38, 39] based on chalcogenide SnS photovoltaic cells, n-ZnO can be taken as a suitable material that can be used as ETL for efficient chalcogenide tin mono-sulfide - based solar cell devices owing to its high stability, proper energy band configuration, and its high light transmittance, electrical conductivity as well as it is costeffective and its element (Zn, O) are non-toxic in nature [5, 40].

In our present work, the designing and simulation of a heterostructure solar cell FTO/n-ZnO/SnS/ $\text{Sb}_2\text{S}_3/\text{Au}$ are performed on SCAPS-1D (v3.3.10) software. In this designed solar structure, SnS is chosen as absorber layer, Sb_2S_3 as HTL, and n-ZnO as ETL. In this study, the impact of shallow acceptor density of SnS absorber and Sb_2S_3 HTL, shallow donor density of n-ZnO ETL, the thickness of HTL, ETL, absorber layer and operating temperature on photovoltaic cell parameters V_{oc} , J_{sc} , FF (%) and η (%) of chalcogenide tin mono-sulfide-based solar cell are studied and analyzed to achieve a better cell performance. Various experimental studies have been reported for different contact electrodes in solar cell application [41–43]. In this study, the observation of the performance parameters of heterojunction photovoltaic cell by altering the different metal back contacts is also studied.

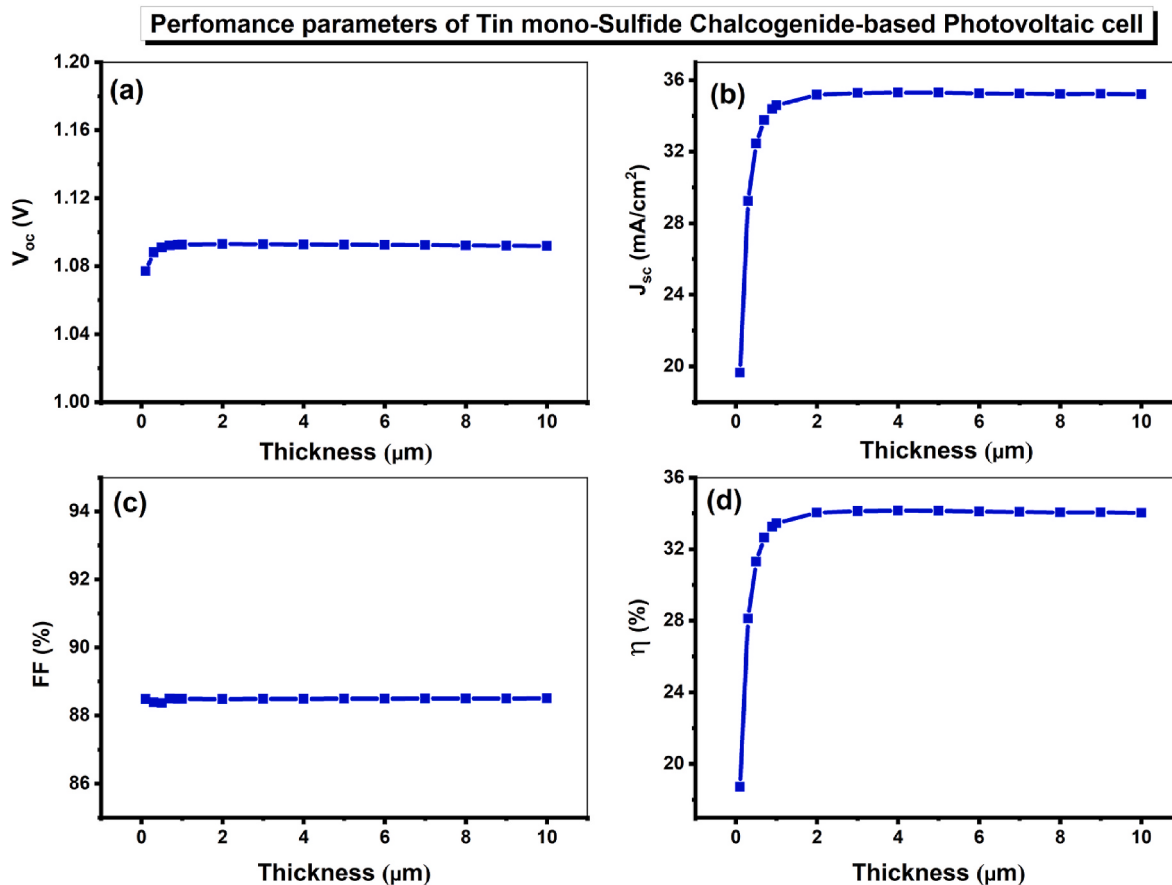


Fig. 4. (a-d): Effect of thickness of SnS absorber on output parameters such as V_{oc} , J_{sc} , FF, and η of Photovoltaic cell.

2. Numerical simulation and Device structure of modeled heterojunction Photovoltaic cell

At present time, the designing of a suitable structure with controlled dimensions best fit for the desired results and analysis of the results of a designed structure can be easily done by numerical simulation methods. The numerical simulation methods provide the control to alter any or many dimensions and constituents of the device to achieve the desired material or device properties. Moreover, numerical simulation methods develop the understanding on the effect of the diverse parameters in designing of a particular device and results without putting any efforts on experimental arrangements since, the experiments require a sophisticated laboratory with a good strategy, much time, energy, resources, and use of chemicals etc. Top on that, only experiment may not give the anticipated results, then experimental iteration method is required for approximation which obviously multiply the requirement of inputs as discussed above. Whereas, in case of numerical simulation methods, these requirements and inputs need not to arrange at the initial level for iteration and approximation. The results obtained by numerical simulation are almost close to the experimental values, so, only final experiment needs to run in the laboratory for further results verification of results and application [44–48]. However, to authenticate the experimental results the repetition of final experiment and on adjacent parameters are always required. In this report, the designing of photovoltaic cell and study of its electrical and optical properties for getting good PCE are being carried out by using one-dimension solar cell capacitance simulator (SCAPS-1D version 3.3.10) software. SCAPS-1D is a worldwide known and a consistent application for photovoltaic device simulation studies, developed by the Department of Electronic and Informative Systems (ELIS) of the University of Gent, Belgium [49]. SCAPS-1D was exclusively designed to investigate the cell performance

of CuInSe₂ and the Cd-Te group. SCAPS-1D has many features that enable one to analyze the different types of solar cells. SCAPS-1D stands out from other similar software due to its user-friendly interface and wide range of defect models, which enable researchers to investigate various device parameters. These parameters include open-circuit voltage (V_{oc}), short-circuit current density (J_{sc}), fill factor (FF), and photo conversion efficiency (PCE). Moreover, SCAPS-1D allows for studying these parameters under different lighting conditions, both in light and dark environments, as well as at different illuminations and temperatures. The software is also suitable for analyzing the performance of both crystalline solar cells (such as those made of Si and GaAs) and thin film solar cells. And it works on the application of Poisson's expression, hole continuity, and electron continuity charge carriers. The software offers the benefit of incorporating up to seven layers of semiconducting materials with different defect properties [50,51].

In order to simulate sun light capture, electron-hole pair creation, extraction, and transportation of charge carriers, SCAPS makes use of important equations. Input of a varied range of exclusive material parameters is enabled by this versatile tool to fabricate solar devices; simulated results are then used to evaluate the effect on photovoltaic device action and gather critical deeps into the vital photovoltaic cell characteristics, including the density of material defects, site and level, recombination, band alignment of device layers with bandgaps, and many more. Overall, SCAPS permits an excess of questions in semiconductor device physics and materials science to be responded.

The Poisson expression for a semiconducting material can be written as –

$$\nabla^2\phi = \frac{q}{\epsilon} (n - p + N_A + N_D) \quad (1)$$

Here, N_A and N_D represent the concentrations of acceptor density and

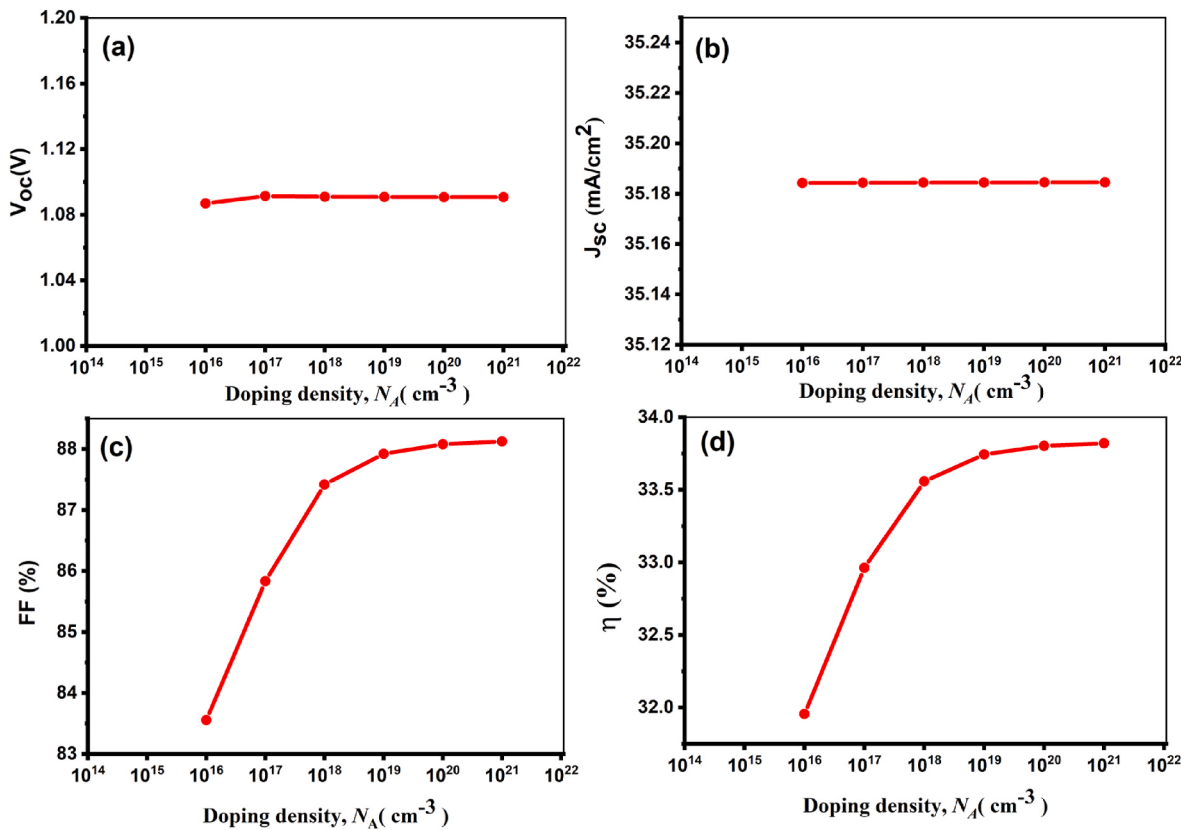


Fig. 5. (a-d): Effect of doping density of HTL Sb_2S_3 on output parameters such as V_{oc} , J_{sc} , FF, and η of chalcogenide tin-mono sulfide-based heterojunction photovoltaic cell.

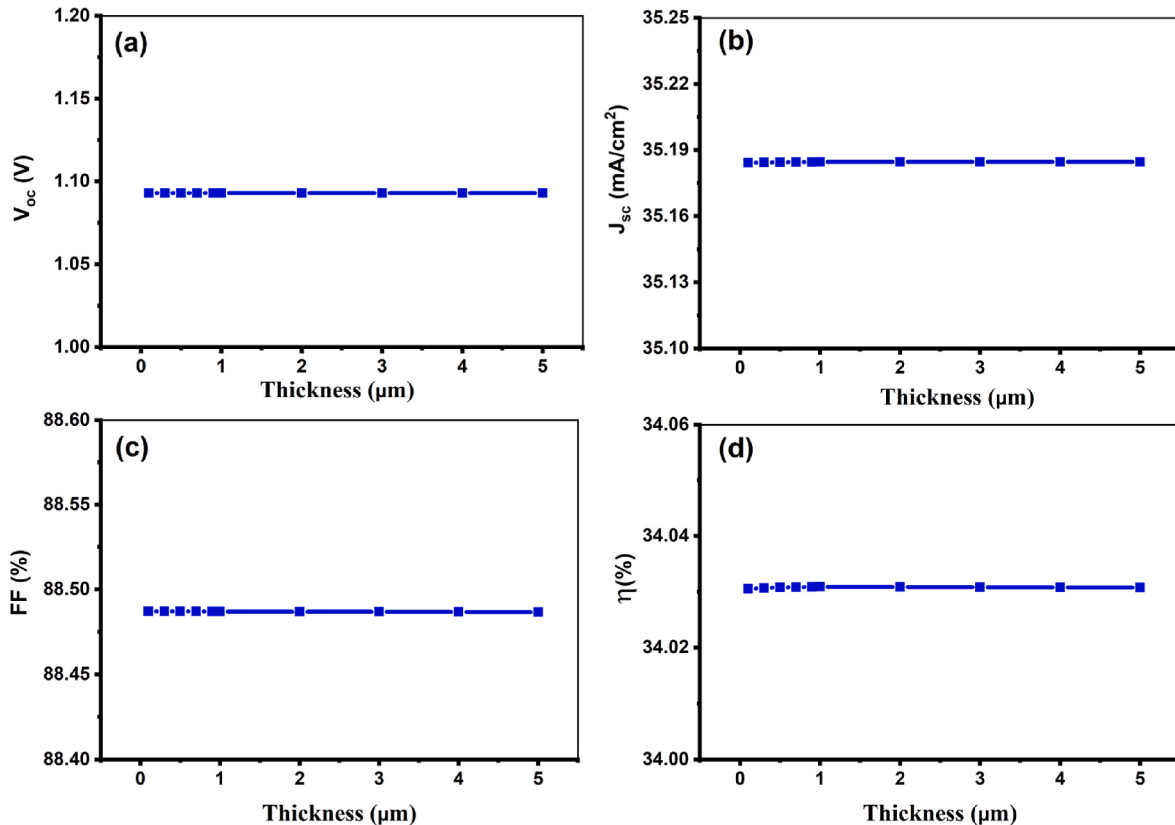


Fig. 6. (a-d): Effect of thickness of HTL Sb_2S_3 on output parameters such as V_{oc} , J_{sc} , FF, and η of chalcogenide SnS-based heterojunction photovoltaic cell (HPVC).

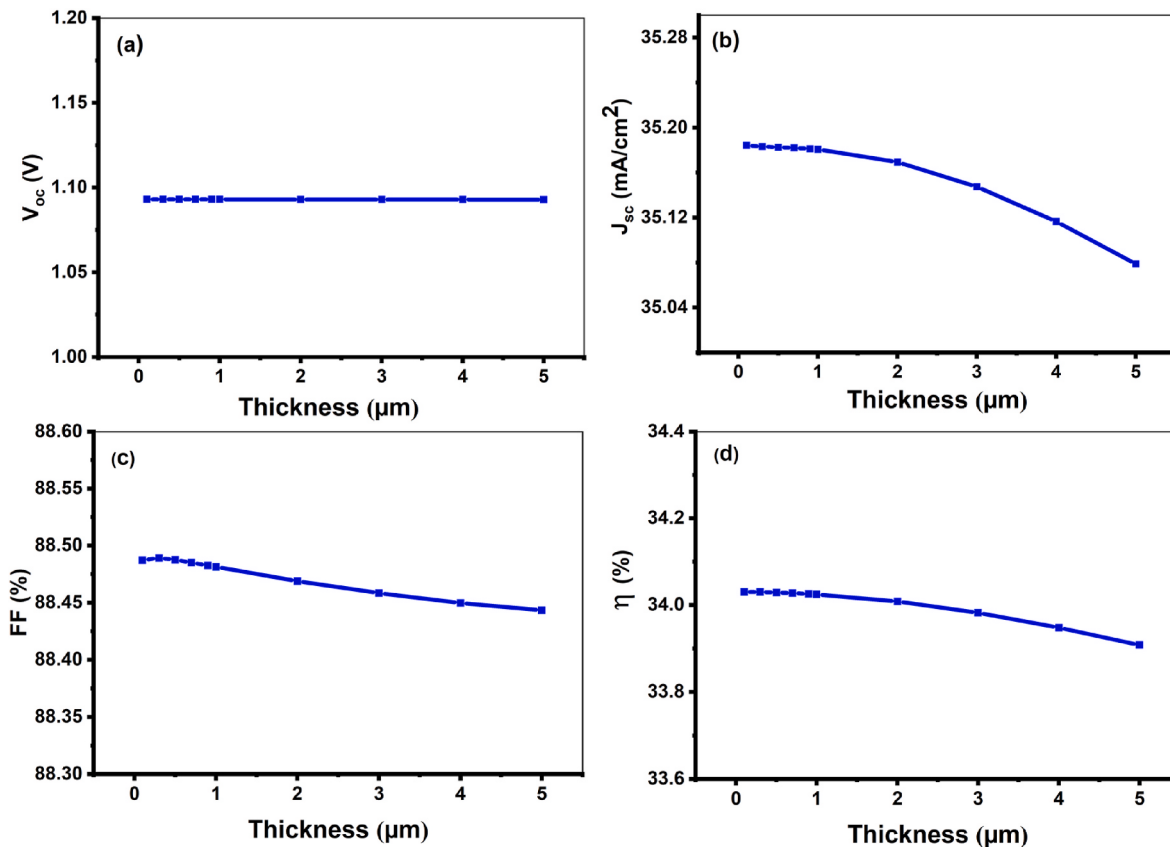


Fig. 7. (a-d): Effect of ETL thickness on output parameters such as Voc, Jsc, FF, and η of chalcogenide tin mono sulfide-based heterojunction photovoltaic cell (HPVC).

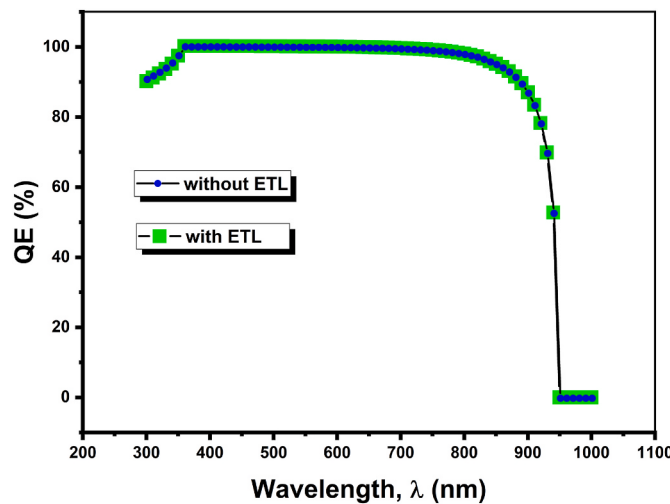


Fig. 8. Variation in quantum efficiency as a function of wavelength of chalcogenide tin-mono sulfide-based heterojunction photovoltaic cell (HPVC) with and without ETL.

donor density respectively, the function φ depicts the electrostatic potential, ϵ is dielectric constant, and p and n are free charge carrier concentration for holes and electrons respectively.

For a semiconducting material, the continuity expression is defined as –

$$\nabla J_n - q \frac{\partial n}{\partial t} = +qR \quad (2)$$

$$\nabla J_p + q \frac{\partial p}{\partial t} = -qR \quad (3)$$

where J_n and J_p are representing current densities for electrons and holes respectively, and R represents the carrier recombination rate. Overall, the current flowing in a semiconductor has two effects, the first one, have drift of minority charges carrier due to the effect of an electric field, and other one is the diffusion current produced due to concentration gradient.

The drift diffusion current relation is represented by continuity equation as –

$$J_n = qn\mu_n\epsilon + qD_n \frac{dn}{dx} = q\mu_n \left(n\epsilon + \frac{kT}{q} \frac{dn}{dx} \right) = \mu_n n \frac{dE_{Fn}}{dx} \quad (4)$$

$$J_p = qp\mu_p\epsilon + qD_p \frac{dp}{dx} = q\mu_p \left(p\epsilon + \frac{kT}{q} \frac{dp}{dx} \right) = \mu_p p \frac{dE_{Fp}}{dx} \quad (5)$$

Here, D_p and D_n are diffusion coefficients of holes and electrons, respectively, μ_n and μ_p are electrons and hole mobility; J_n and J_p are electron and holes current density; and E_{Fn} and E_{Fp} are Quasi-Fermi level for electrons and holes respectively [52–54]. For interference recombination, SCAPS-1D software uses the Pauwells-Vanhoutte model [51], which consider the conduction and valence bands of both semiconductor on the interference.

In this report, all simulation has been performed by using the illumination of A.M_1.5_1_sun.spe (Air Mass 1.5 Global Spectrum) sun light spectrum with an incident power density of 1000 W m^{-2} [55,56]. In SCAPS-1D program, we can give input up to seven semiconductor layers excluding front and back contact for the simulation study we have used. For every layer, the basic material parameters (Table 1) for simulation were given in SCAPS-1D (v3.3.10) definition panel. The device

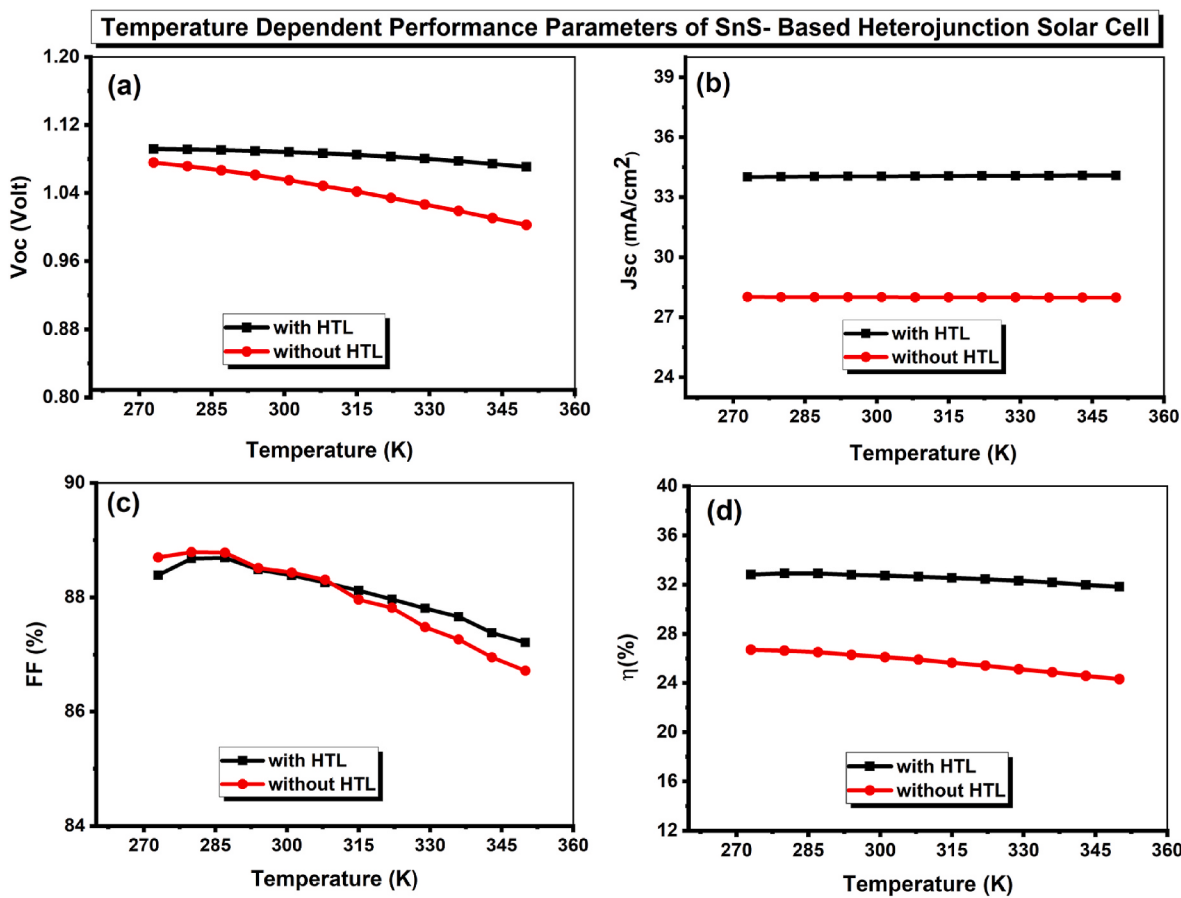


Fig. 9. (a-d): Effect of temperature with and without Sb_2S_3 HTL on chalcogenide tin-mono sulfide-based heterojunction photovoltaic cell (HPVC).

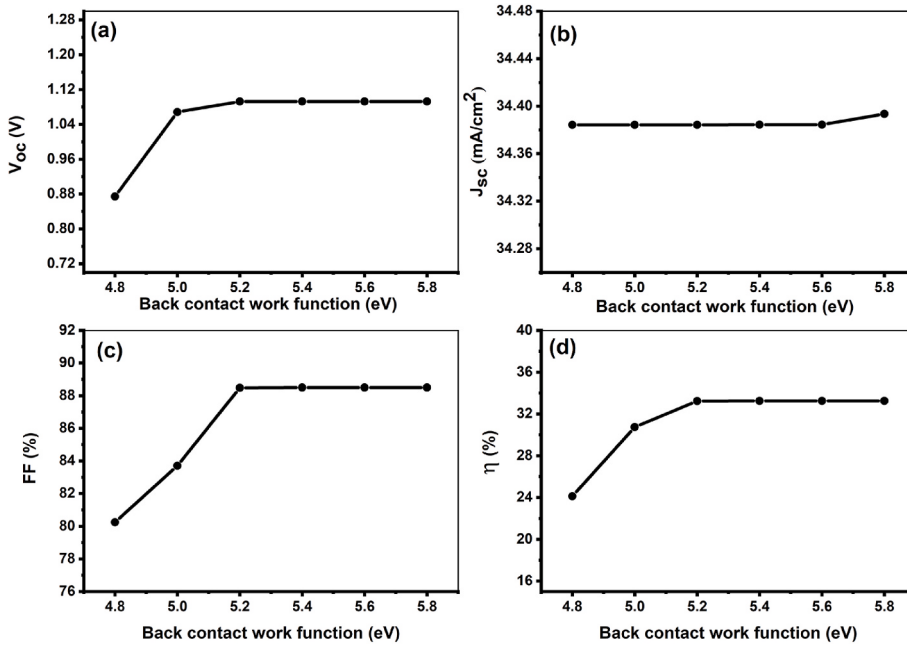


Fig. 10. (a-d): Effect of back contact work function on chalcogenide tin-mono sulfide-based heterojunction photovoltaic cell (HPVC).

architecture is FTO/n-ZnO/SnS/ Sb_2S_3 /Au. The first layer in the device is Sb_2S_3 as HTL, second layer is SnS as absorber layer, third layer is n-ZnO as ETL, fourth layer is FTO as transparent conducting oxide (TCO) which also works as front contact (metal work function 4.4 eV) [57] and Au

(Gold) as back contact (of metal work function 5.2 eV) [58,59].

The schematic of photovoltaic device structure, energy band alignment diagram and energy band diagram of chalcogenide tin mono sulfide-based modeled heterojunction photovoltaic cell (HPVC) with

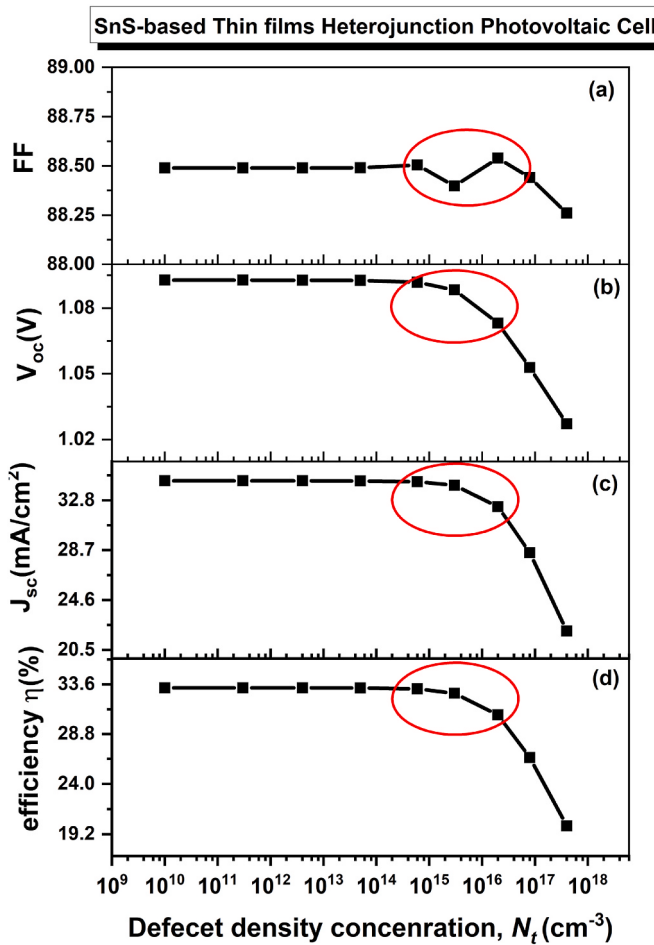


Fig. 11. (a-d): Effect of Defect concentration of absorber on chalcogenide tin-mono sulfide-based heterojunction photovoltaic cell (HPVC).

Sb_2S_3 HTL are depicted in Fig. 1(a-c).

From Fig. 1(c), the staggered band alignment and cliff formed at the interface of SnS and Sb_2S_3 is an exemplary condition for the movement of holes and interception of electrons.

3. Results and discussion

3.1. Effect of Sb_2S_3 as HTL on the performance of SnS-based heterojunction photovoltaic cell

In this simulation study, the values of basic electrical parameters of designed photovoltaic heterostructure are highlighted in Tables 1 and 2 [28,32,60–63]. We have two kinds of chalcogenide tin mono sulfide-based heterojunctions, one is with HTL and another is without HTL. To examine the role of HTL Sb_2S_3 in SnS-based photovoltaic (PV) cell, we have analyzed the simulated results based on the J-V characteristic. Fig. 2 (a) exhibits the current density - voltage (J-V) curves of the chalcogenide tin mono sulfide-based thin film HPVCs with and without HTL.

It can be seen from Fig. 2(a) that the observed current density of the designed FTO/ZnO/SnS/ Sb_2S_3 /Au HPVC is implicitly more in comparison to that of a reference chalcogenide SnS-based thin film HPVC of FTO/ZnO/SnS/Au. The different parameters associated to TCO, absorber layer, ETL and HTL as recorded in Table 2, are kept constant while we remove the HTL to analyze the solar cell performance.

The photovoltaic cell performance parameters taken out from J-V curve of both heterostructures are tabulated in Table 3. We can observe from Fig. 2 (a) that the current density and voltage characteristics of the

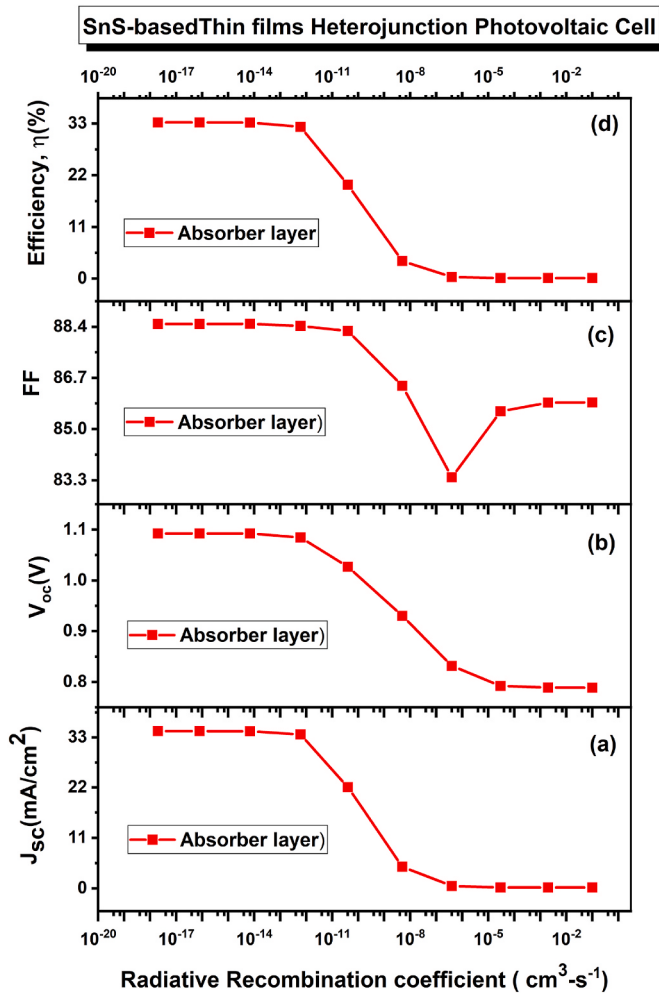


Fig. 12. (a-d): Impact of radiative recombination coefficient on chalcogenide tin-mono sulfide-based heterojunction photovoltaic cell (HPVC).

heterojunction comprising HTL Sb_2S_3 are much improved than the heterojunction without HTL. The output parameters of these two structures are determined to be $V_{oc} \sim 1.05 \text{ V}$, $J_{sc} \sim 27.99 \text{ mA/cm}^2$, and $FF \sim 88.44 \%$, and $\eta \sim 26.15 \%$, whereas the values of optimized parameter of HPVC viz. V_{oc} , J_{sc} , FF and η are 1.09 V , 34.38 mA/cm^2 , 88.49% , and 33.24% respectively.

Fig. 2 (b) illustrates the quantum efficiency (QE) curves against the wavelength range (300–1000 nm) of radiation used for proposed designed photovoltaic cell structures with and without HTL.

The sudden reduction in the QE is detected at the wavelength confirming the energy band gap close to $\sim 1.32 \text{ eV}$ for SnS active absorber layer. We can see that the heterostructure with HTL have high QE in comparison to heterostructure without HTL in long range of wavelength. High QE may be attributed to the photo generated charge carriers owing to electric field generation at back surface. SnS and Sb_2S_3 have very high absorption rate of energy of photons with lower wavelength and the poor recombination rate in these layer sections of photovoltaic cell might lead to much improved conversion efficiency. This QE behavior may be the result of loss of minority charge carriers and low surface recombination at SnS/ Sb_2S_3 interface [32,34]. The Sb_2S_3 and SnS form a $p^+ - p$ high-low junction and avert the minority charge carrier's recombination loss at the interface. This could be the possible reason for the substantial enhancement in the output performance parameters of designed photovoltaic cell.

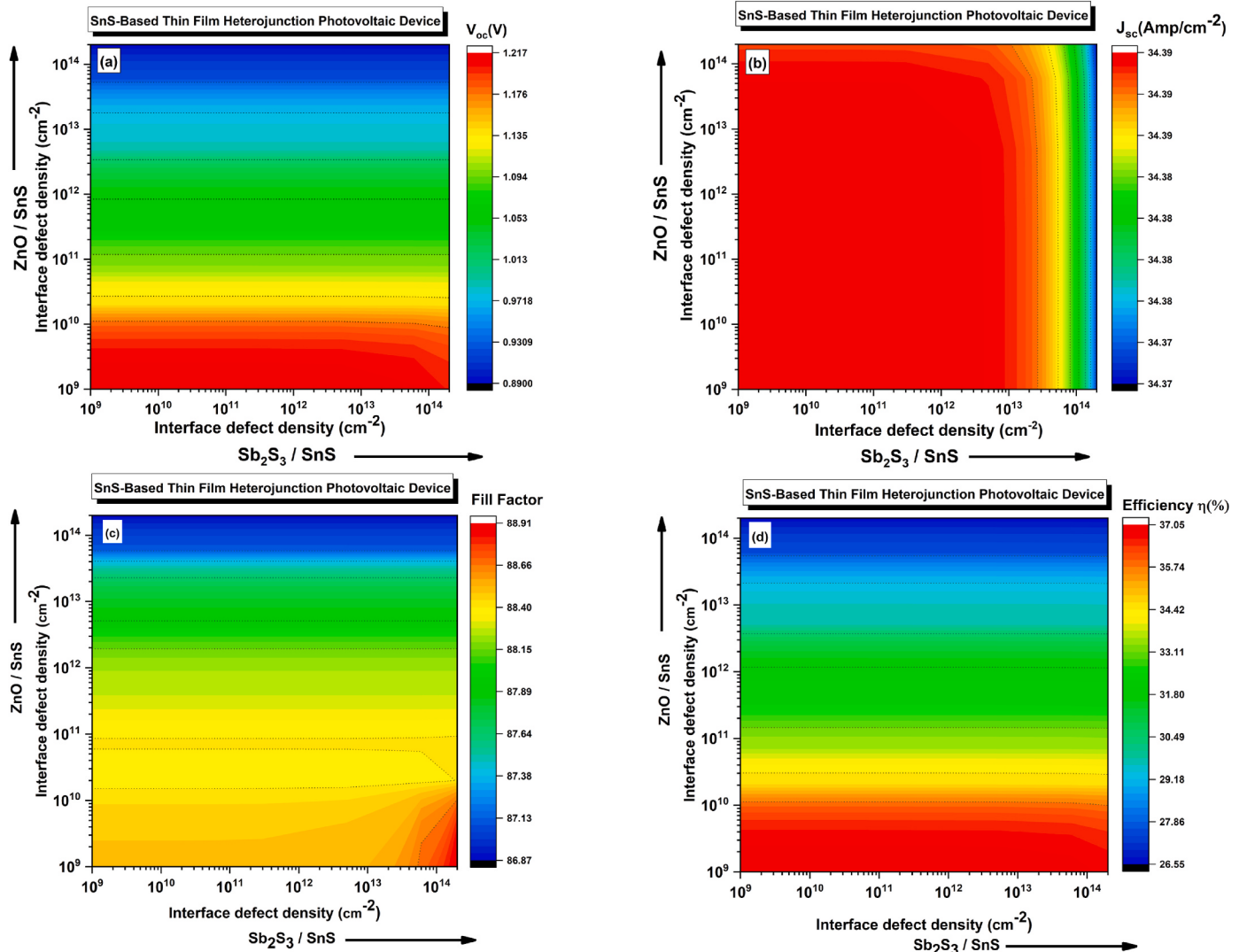


Fig. 13. (a-d): Effect of Interface defect density on chalcogenide tin-mono sulfide-based heterojunction photovoltaic cell (HPVC).

3.2. Impact of doping density and thickness of chalcogenide tin mono sulfide absorber on heterojunction photovoltaic cell

To design an efficient photovoltaic cell, it is imperative to determine the shallow acceptor density and thickness of absorber layer. As photo-generated charge carriers in the absorber layer play a vital role in analyzing the performance of photovoltaic cell. Herein present work we have examined the impact of absorber layer by varying shallow acceptor density and thickness. Fig. 3(a-d) illustrates the simulation study on performance results of heterojunction photovoltaic cell against shallow acceptor density of absorber. The shallow acceptor density, N_A is varied from 10^{16} to 10^{21} cm^{-3} and it is observed that the resultant parameters of the photovoltaic cell for lower acceptor density lying between 10^{16} - 10^{18} cm^{-3} , are almost zero, which could be due to auger recombination and hole transportation was suppressed by HTL owing to rise of scattering contamination and rate of recombination is very high. But when the carrier concentration is reached order of $\sim 10^{19} \text{ cm}^{-3}$ then, J_{sc} is almost constant, V_{oc} sharply increases, the value FF increases slightly. As a result, the value of η for photovoltaic cell sharply enhances, it may be due to an increase in acceptor density, and thus, the density of hole carriers increases which leads to high mobility of electrons and charge carrier generation. For the formation of $p^+ - p$ type heterojunction and for optimum performance of photovoltaic cell the shallow acceptor density, N_A is considered $\sim 10^{20}$ per cm^3 for SnS absorber layer [68].

Fig. 4(a-d) illustrates the consequence of the thickness variation of chalcogenide tin mono sulfide absorber layer on the output performance parameters of HPVC. The thickness is ranged between 10 nm and 10 μm while putting the all-other parameters fixed. It can be observed from figure that the value of J_{sc} increases sharply till 900 nm, open circuit voltage gradually increases till 900 nm, thereafter at 2 μm both the parameters get saturated. It can be explained that the increase in the thickness, the absorption of photons in the absorber layer increases which leads to the generation of electron-hole pair with high electron mobility, current density, and carrier generation. The fill factor almost remains constant, which results in a sharp increase in efficiency till 900 nm, thereafter it gets saturated [64].

The tin mono sulfide absorber layer gets saturated at 2 μm and gives efficiency of 34.10 % but to reduce the needed amount of raw material, so the material cost gets decreased from a practical application point of view, and with increase in thickness recombination increases in some cases, so we have taken SnS absorber layer thickness to be 0.90 μm [24]. Hence, the optimal value of η is ~ 33.04 % at HTL shallow acceptor doping density of $\sim 10^{20}$ per cm^3 and the optimal thickness for the layer is $\sim 0.90 \mu\text{m}$. These values of doping concentration and thickness are set as optimized physical parameters for the absorber layer in achieving better cell performance.

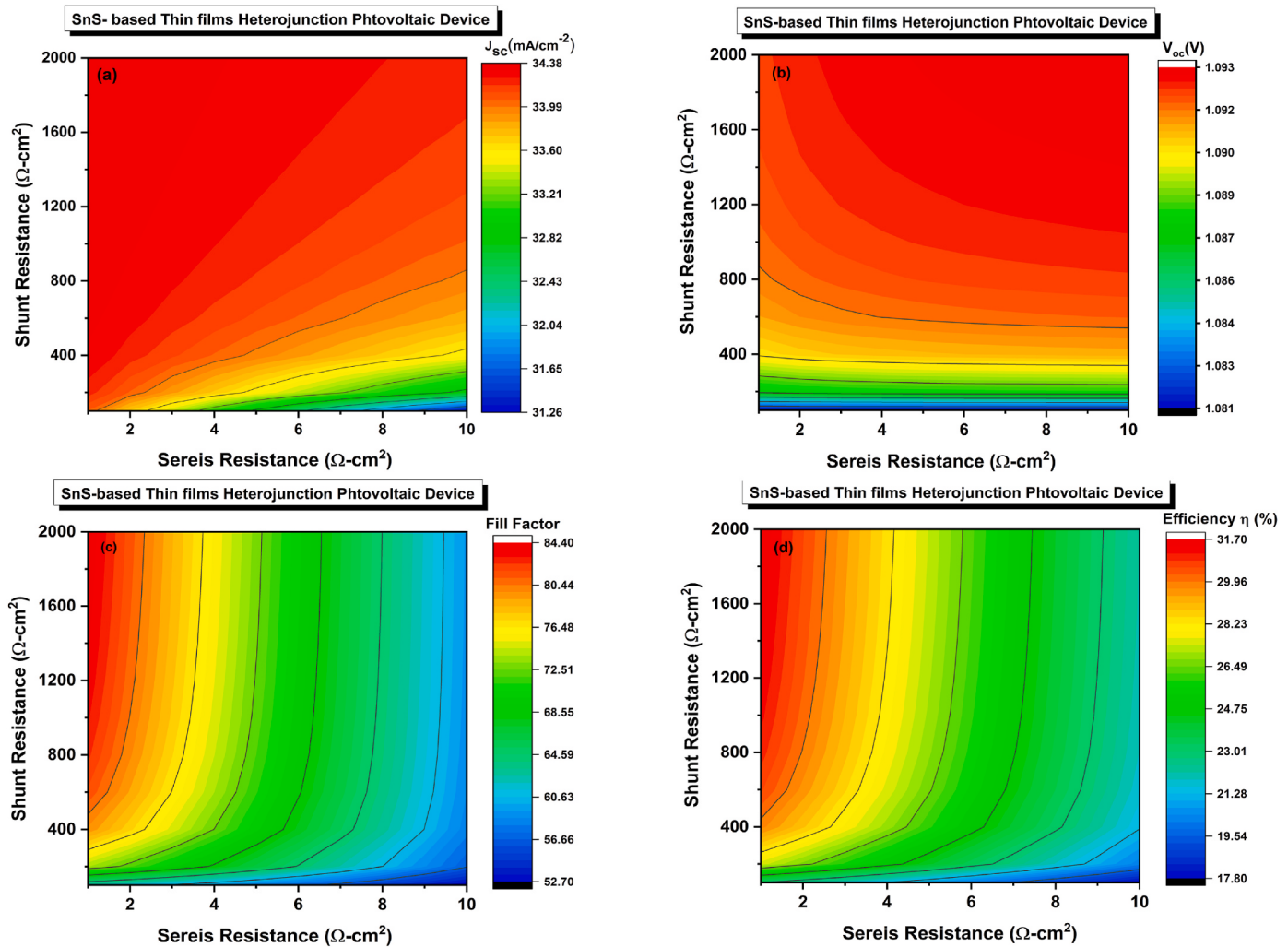


Fig. 14. (a-d): Impact of Series and Shunt resistances on chalcogenide tin-mono sulfide-based heterojunction photovoltaic cell (H).

3.3. Impact of doping density and thickness of Sb_2S_3 active HTL on heterojunction photovoltaic cell

For improved performance of the photovoltaic cell, we need HTL to be efficient in the transportation of charge carriers as well as in collection of charge carriers. The active HTL transports the photon generated holes in active absorber layer to the electrode, in addition to it blocks the minority charge carrier (e^-) to reduce the charge carrier recombination in the heterojunction of photovoltaic cell which helps in overall performance of chalcogenide tin mono sulfide - based photovoltaic cell. In this present communication, we have examined the impact of doping density and thickness of HTL on chalcogenide tin mono sulfide - based photovoltaic cell, keeping other parameters fixed. Fig. 5(a-d) illustrates the variation in output parameters of photovoltaic cell as a function of the doping density of HTL.

The shallow acceptor density is varied from 10^{16} to 10^{21} cm^{-3} and we can observe that the J_{sc} is almost unchanged, V_{oc} slightly increased until 10^{18} cm^{-3} then it remains constant, in the range. Overall, based on the changes, the values of fill factor and efficiency increase in a linear fashion up to 10^{18} cm^{-3} thereafter they increase in nonlinear manner till 10^{21} cm^{-3} . It may be accredited to increase in carrier concentration at large doping which leads to move more holes toward the SnS/ Sb_2S_3 interface. The minority electrons do not recombine with all holes in HTL, which improves the values of FF and η [34,65]. In addition, the fill factor improves because of an improvement in resistivity at the interface reducing the series resistance and further increasing conductivity of HTL

with increasing doping density. Furthermore, extensive doping improves the entire charge transfer mechanism by increasing the conductivity of the hole-transport layer. It also offers an ohmic interface between the electrode and HTL, which is required for effective charge collection, and it increases interface resistance by lowering traps in the absorber layer, which is required for efficient hole extraction. The optimized doping of the hole-transport layer can help to tune the energy level between the hole-transport layer and the absorber [68–70].

Fig. 6(a-d) illustrates the variation of output parameters against the thickness of Sb_2S_3 layer for chalcogenide tin mono sulfide - based photovoltaic cell. The thickness of layer is ranged between 10 nm and 5 μm by putting all other parameters remain fixed, we can observe that the all-output performance parameters like V_{oc} , J_{sc} , FF, and η of the proposed heterojunction remain approximately constant [65,66]. Hence, the optimal value of $\eta \sim 33.24 \%$ at HTL doping concentration of 10^{21} per cm^3 along with thickness of 0.100 μm is assessed, and these doping shallow acceptor density and thickness are put as improved physical parameters for HTL in ensuing photovoltaic cell performance calculation.

3.4. Impact of thickness of n-ZnO ETL on chalcogenide tin mono sulfide-based heterojunction photovoltaic cell

In this report, we have used n-ZnO as an ETL in SnS based solar cell. Fig. 7(a-d) illustrate the thickness impact of n-ZnO on SnS- based solar cell. The thickness is ranged between 10 nm and 5 μm while keeping the

Table 4

Comparison of photovoltaic performance parameters for chalcogenide tin-mono sulfide-based and Sb_2S_3 -based heterojunction photovoltaic device.

Structures	Type of study	Photovoltaic performance parameters			
		V_{oc} (V)	J_{sc} (mA/cm ²)	FF (%)	η (%)
TCO/CdS/SnS-Cubic/SnS-Orth/Contact [83]	Exp.	0.488	6.96	41	1.38
SLG/Mo/SnS/CdS/i-ZnO/ZnO:B/Ni/Ag [84]	Exp.	0.269	13.28	45.07	1.61
Glass/Mo/SnS/CdS/i-ZnO/Al/ZnO/Ni/Al [2]	Exp.	0.28	20.3	40	2.28
SLG/Mo/SnS/CdS/i-ZnO/AZO/Ni/Ag [85]	Exp.	0.297	19.4	52.8	3.05
SLG/Mo/SnS/CdS/i-ZnO/AZO [86]	Exp.	0.334	18.9	55.5	3.50
Glass/Mo/SnS/SnO _x /Zn(O, S):N/ZnO/ITO [3]	Exp.	0.372	20.2	58	4.36
TiO ₂ /n-Sn/SnS/Ag/SnS-p-SnS/ITO [87]	Exp.	0.45	17.13	68	5.24
FTO/CdS/Sb ₂ S ₃ /(Au, Ag) [88]	Exp.	0.52	9.52	48	2.38
FTO/CdS/Sb ₂ S ₃ /Au [89]	Exp.	0.59	10.92	46.77	3.02
Contact/n-ZnO/n-CdS/p-SnS/Contact [90]	Simul.	0.752	33.29	62	15.62
Contact/p-SnS/CdS/ZnO/Contact [91]	Simul.	0.92	13.4	86.3	10.6
AZO/ZnO/CdS/Sb ₂ S ₃ /Au [92]	Simul.	1.23	20.15	83.1	20.6
Mo/Sb ₂ S ₃ /CdS/i-ZnO/ZnO/Al/metal contact [28]	Simul.	0.72	15.98	83.23	9.52
Glass/Mo/SnS/SnO _x /Zn(O, S):N/ZnO/ITO [5]	Simul.	0.419	27.99	67.97	7.68
Glass/ITO/ZnO/CdS/SnS/Contact [22]	Simul.	0.732	20.75	36.89	8.92
Present work					
FTO/n-ZnO/SnS/Sb ₂ S ₃ /Au	Simul.	1.09	34.38	84–88	30–33

other different parameters fixed, we can observe that the all-output parameters like J_{sc} , V_{oc} , FF, and η of projected heterojunction remain approximately constant [71]. For further influence of ETL on chalcogenide tin mono sulfide-based heterojunction photovoltaic cell, we have studied the impact of ETL on quantum efficiency as a function of wavelength of sun's spectra for two designed different photovoltaic structures with ETL and without ETL (see Fig. 8). The wavelength is varied from 300 to 1000 nm. There is no noticeable variation for with and without ETL. The current generated due to insufficient photoinduced charge carriers along with slightly wider ETL might be the explanation for the stability of the proposed heterojunction [72]. Hence, the optimal thickness of ETL $\sim 0.100 \mu\text{m}$ with $J_{sc} \sim 34.38 \text{ mA/cm}^2$, $V_{oc} \sim 1.09 \text{ V}$, FF $\sim 88.49 \%$, and $\eta \sim 33.24 \%$ is estimated.

3.5. Impact of temperature, and rear contact metal work function on chalcogenide tin mono sulfide-based heterojunction photovoltaic cell

The temperature at which the photovoltaic cell, is operating, plays a vital role on the output parameters of the photovoltaic device. In this report, we have set a range for the operating temperature between 273 K and 350 K for the heterojunction with or without HTL. Fig. 9(a–d) illustrates the variation of heterojunction with temperature. The values of V_{oc} and FF decreases linearly and J_{sc} has minor increment, as a result, the efficiency decreases linearly with increase in temperature. It may be due to the generation of sufficient pair of electron and hole at high temperatures which leads to recombination of charge carriers and thus, decrease in V_{oc} .

As the temperature rises the energy band gap decreases of semiconductor which leads to a small rise in the J_{sc} [73–75]. These combined effects of V_{oc} and J_{sc} lead to decrease in fill factor and efficiency, but due

to its proper band alignment, the PCE of chalcogenide tin mono sulfide-based photovoltaic cell with HTL at temperatures 273K and 350K are 33.29 % and 31.8 % respectively [34] whilst, for the case of without HTL the PCE at 273K and 350K are 26.69 % and 24.32 % respectively. Hence, we can conclude that the optimal performance of chalcogenide tin mono sulfide-based photovoltaic cell with HTL Sb_2S_3 at 273K has better stability.

The back metal contact of FTO/n-ZnO/SnS/Sb₂S₃/Au heterojunction also plays an important role on tin-sulfide (SnS) chalcogenide-based heterojunction photovoltaic cell (HPVC). Fig. 10(a–d) illustrates the back metal contact impact on chalcogenide tin mono sulfide-based photovoltaic cell. Different materials for rear contact are utilized for the optimization of the performance of HPVC. The values of work function of different rear metal contacts are ranged between 4.8 and 5.8 eV while keeping the different parameters constant [76].

The values of V_{oc} , FF, and η increase significantly until 5.2 eV, then it is saturated. It may be due to the potential barrier generated by majority of charge carriers at the interfacial boundary of Sb_2S_3 /rear metal contact reduces with increase in rear metal contact work function which leads to increase in the performance of photovoltaic cell. The short circuit current density slightly changes at 5.6 eV which is compatible with the study [77]. The result concludes that the rear metal contact work function should be more than 5.2 eV like metals Au, Ag, Ni, Pt, and Pd for optimum performance of photovoltaic cell. In the present modeled device structure, we have used Au as a back metal contact [78–80].

3.6. Impact of defect concentration of absorber layer on chalcogenide tin-mono sulfide-based heterojunction photovoltaic cell

The condition of an active absorber layer significantly influences photovoltaic energy conversion. Having a large defect concentration in the active layer could increase the carrier recombination rate and, consequently, lower the overall performances of the photovoltaic cell. In this current study, the impact of the defect concentration of chalcogenide tin-mono sulfide-based active absorber layer on the cell performance is examined. There are various types of defects in tin-sulfide, such as acceptor and donor vacancies, antistites, and interstitials.

There is little information available about all types of defects in chalcogenide tin-mono sulfide-based systems. The SCAPS simulation allows dissimilar donor and acceptor defects to be introduced, but we choose to introduce only a single acceptor-like defect in the chalcogenide tin-mono sulfide-based p-type active layer owing to the lower creation energy of acceptor density of defects in comparison to donor ones. Fig. 11(a–d) exemplify the variation of defect density of tin-sulfide absorber on performance parameters of photovoltaic device. The consequence of defect density in between the range of 10^{10} – 10^{18} per cm³ is studied to determine the performance of photovoltaic cell. We can perceive that the performance of photovoltaic cell does not alter up to the defect density is below 3×10^{15} per cm³. It is clear from Fig. 11(a–d) that the performance parameters of PVC are commenced decreasing on further increasing the value of defects concentration beyond 10^{15} cm^{−3}. Although a slight down in the value of fill factor is noticed at 3×10^{15} cm^{−3}, beyond it, the value of FF slightly increased and on further exceeding the defect concentration in the active absorber layer, declined the result of FF. Overwhelmingly, when the density of defect is lower than the value $\sim 10^{16}$ per cm³, the large noticed PCE is greater than 33 %, short circuit current density is observed 34.40 mA/cm^2 whereas the $V_{oc} \sim 1.09 \text{ V}$ but the value of fill factor for optimized density 3.0×10^{15} cm^{−3}, is noticed ~ 88.50 . Thus, it is clear from above results that the defect concentration in the highly thick active absorber layer has a contrary consequence on the performance of chalcogenide mono tin sulfide-based HPVC. The value of defect concentration 3×10^{15} cm^{−3} is utilized as an optimized physical parameter for absorber layer in subsequent HPVC performance evaluation of the present modeled device structure.

3.7. Impact of radiative Recombination coefficient on chalcogenide tin-mono sulfide-based heterojunction photovoltaic cell

The value of rate of radiative recombination is primarily determined by the atomic configuration and charge carrier density of the film, which directly influence V_{oc} of the photovoltaic device [81]. In this present work, simulation was performed by varying the value of rate of radiative recombination coefficient in the range of $10^{-18} \text{ cm}^3 \cdot \text{s}^{-1}$ to $10^{-1} \text{ cm}^3 \cdot \text{s}^{-1}$. It is clear from Fig. 12(a-d) that the value of performance parameters of heterojunction photovoltaic cell gives maximum results corresponding to the radiative recombination value lower than the $10^{-14} \text{ cm}^3 \cdot \text{s}^{-1}$. It is also found that each performance parameter displays variation as a function of radiative recombination coefficient (RRC) for larger than $10^{-14} \text{ cm}^3 \cdot \text{s}^{-1}$ value. They are decreased on increasing the values of RRC. It is due to the rapidly declining the value of generated carrier collection on increasing the recombination rate [82].

Overall, the optimized values of performance parameters especially PCE is noticed more than 33 %, short circuit current density is observed 34.40 mA/cm^2 however the $V_{oc} \sim 1.09 \text{ V}$ and the value of fill factor is noticed ~ 88.50 associated with the value of RRC $< 10^{-14} \text{ cm}^3 \cdot \text{s}^{-1}$. The performance analysis for this section, the earlier acquired optimized results are considered.

3.8. Impact of Interface defect states on SnS-based heterojunction photovoltaic cell

Interface defects act as recombination centres, and they are triggered by band alignment, misfit dislocations, and secondary phases. Therefore, interface defect states have a substantial role on the performance of photovoltaic devices. In this present communication interface defect study of designed photovoltaic structure is carried out in the range 10^9 to 10^{14} cm^{-2} . The interfaces of tin sulfide-based photovoltaic device SnS/Sb₂S₃ and n-ZnO/SnS. To examine the influence of interfacial defect density for the performance of photovoltaic device at absorber/HTL and ETL/absorber interfaces, the neutral defect densities at these interfaces were varied in according aforementioned range.

The performance analysis of the photovoltaic device from the numerical simulation in this segment was carried out by considering the earlier acquired optimized results. A graphical contour plot representation is depicted in Fig. 13(a-d). It can be understood from figure that all the photovoltaic device performance parameters were nearly unchanged in the range of 10^9 - 10^{14} per cm^2 for the active absorber/HTL interfacial boundary but the values of FF, η and V_{oc} , were significantly changed and J_{sc} is independent from the variation of defect density at the ETL/absorber interfacial boundary. It is clear from the contour diagram that the result of V_{oc} reduces from 1.21 to 0.89 V with increasing the defect density in the range 10^9 - 10^{14} cm^{-2} , whereas fill factor and efficiency are declined from 88.91 to 86.88 % and 37 %–26.6 % respectively.

It can be accredited to more recombination centres and traps produced by the larger value of density of defects associated to the buffer/absorber interfacial region which leads to deprivation of the photovoltaic cell's performance. Finally, from above simulated outputs, this can be specified that the density of defect variation close to the buffer/absorber interfacial region has significant impact on the photovoltaic device performance in comparison to the defect variation at the absorber/HTL interfacial boundary. To attain the optimum performance for the projected chalcogenide tin-mono sulfide-based thin film photovoltaic device structure, the interfacial defect density of value $\sim 10^{11} \text{ per cm}^2$ is considered at both active interfacial boundaries.

3.9. Impact of parasitic series, and Shunt resistances on chalcogenide tin-mono sulfide-based heterojunction photovoltaic cell

In PV devices, the series and shunt resistances have a vital impact on performance. Series resistance, R_s is primarily derived from the contact

between the multiple junctions and the metal rear and front contacts used in heterojunction photovoltaic devices. Meanwhile, the reverse saturation current of the energetic junction owing to engineering defects of photovoltaic devices generates the shunt resistance, R_{sh} . In order to modeled and manufacture high-performance photovoltaic devices, it is necessary to attain poor series resistance and high shunt resistance of devices. The impact of R_s and R_{sh} on the performance of a photovoltaic device including Sb₂S₃ HTL is inspected utilizing the SCAPS-1D simulator in the present communication. In order to evaluate the influence of R_s and R_{sh} , we held all other improved parameters at their optimal values from the previous section.

Fig. 14(a-d) shows the gained contour plot of the modeled photovoltaic device performance parameters with J_{sc} , V_{oc} , FF, and η as the series resistance and shunt resistance fluctuate from 1 to $10 \Omega \cdot \text{cm}^2$ (on the x - axis) and from 10^2 to $2.0 \times 10^3 \Omega \cdot \text{cm}^2$ (the y - axis), respectively. The open circuit voltage (V_{oc}) displays quite slow dependence only on smaller values of R_{sh} in comparison to R_s however the short circuit current density (J_{sc}) is subtle to the larger values of R_s compared to the R_{sh} (refers Fig. 14(a-b)). Fig. 14(c-d) exemplifies that both the FF and η are noticeably changed with respect to the variation of R_s and R_{sh} . It can be observed from contour diagram Fig. 14(c-d) that as a function of R_s , the FF and η decline from 81.3 to 59.2 % and from 31.7 % to 22.1 % correspondingly.

Likewise, the FF and η increase from 62.4 % to 84.3 % and from 23 % to 31.7 %, correspondingly, as R_{sh} increases (refer Fig. 14 (c-d)). It may be owing to a lessening the value of leakage current in the projected photovoltaic structure and thereby changing the performance parameters. Consequently, it is disclosed that the variations in the values of R_s and R_{sh} have an excessive impact on the performance of the heterojunction photovoltaic device. Performance parameters are strictly influenced at the low values of series resistance at $1.0 \Omega \cdot \text{cm}^2$ and nearly saturated by R_{sh} higher than $1800 \Omega \cdot \text{cm}^2$, as publicized in Fig. 14(a-d).

3.10. Comparative results of chalcogenide tin-mono sulfide - based heterojunction photovoltaic cell

A comparison of several previous results of investigations of heterojunction photovoltaic cells based on SnS and other active layers (electron-hole transports) is provided in the ensuing Table 4 [2,3,5,22, 83–89]. It can be realized from this study that the calculated efficiency of photoconversion efficiency is high in comparison to theoretical values reported for other heterojunction photovoltaic cells based on SnS.

4. Conclusions

Herein present communication, the performance of chalcogenide tin mono-sulfide absorber comprised photovoltaic cell with a proposed heterojunction structure of FTO/n-ZnO/SnS/Sb₂S₃/Au is studied by a numerical simulation using SCAPS-1D program. The simulation was performed to analyze and evaluate the impact of doping concentration and thicknesses of different active layers viz. absorber, HTL, and ETL, operating temperature, rear back contact's work function, defects, recombination, series, and shunt resistances on the performance parameters of chalcogenide mono tin sulfide-based heterojunction thin film photovoltaic device. Simulated results revealed that the doping carrier density of 10^{20} per cm^3 with a width of $0.90 \mu\text{m}$ for chalcogenide tin-mono sulfide absorber layer, and 10^{21} cm^{-3} with $0.10 \mu\text{m}$ for the chalcogenide Sb₂S₃ HTL and a thickness of $0.10 \mu\text{m}$ for n-ZnO ETL, the maximum power efficiency $\eta \sim 33 \%$ has observed for the proposed HPVC. Furthermore, the variation of defect density of the absorber layer as well as the interfacial defect density of Sb₂S₃/SnS and SnS/n-ZnO is optimized at 10^{15} per cm^3 and 10^{11} per cm^2 respectively, and recorded maximum photoconversion efficiency. The optimized values of series and shunt resistances $1.0 \Omega \cdot \text{cm}^2$ and $1800 \Omega \cdot \text{cm}^2$ have recorded good performance parameters. For chalcogenide tin-mono sulfide-based HPVC an optimized heterojunction structure with performance

parameters viz. $V_{oc} \sim 1.09$ V, $J_{sc} \sim 34.4$ mA/cm², and $FF \sim 84\%$ –88.49%, and $\eta \sim 31\%$ - 33 % are obtained. Overall, the study has shown an improved cell performance of chalcogenide based HPVC with SnS as an absorber when combined with Sb₂S₃ as an HTL. Moreover, the observed simulation results seem encouraging to us, and in terms of future research, an experimental investigation is needed to check the stability and lifetime of the chalcogenide SnS-based cell structure under different weather conditions in real time. SnS-based HPVC could be a useful candidate for the photovoltaic cell community as it is a competent, costefficient, and stable thin film heterojunction photovoltaic cell model.

CRediT authorship contribution statement

Amarjeet Kumar: Writing – original draft. **Rahutosh Ranjan:** Writing – original draft. **Vijay Kumar Mishra:** Writing – review & editing. **Neelabh Srivastava:** Writing – original draft. **Rajanish N. Tiwari:** Writing – review & editing. **Laxman Singh:** Writing – review & editing. **Arvind Kumar Sharma:** Software, Supervision, Writing – original draft.

Declaration of competing interest

The authors declare that they have no conflict of interest.

Acknowledgement

The authors sincerely thank Dr. Marc Burgelman at the department of Department of Electronics and Information Systems (ELIS) of the University of Gent, Belgium and his group providing the SCAPS-1D program.

References

- [1] J.A. Andrade-Arvizu, M. Courel-Piedrahita, O. Vigil-Galán, SnS-based thin film solar cells: perspectives over the last 25 years, *J. Mater. Sci. Mater. Electron.* 26 (7) (Jul. 2015) 4541–4556, <https://doi.org/10.1007/s10854-015-3050-z>.
- [2] V.R. Minnam Reddy, H. Cho, S. Gedi, K.T.R. Reddy, W.K. Kim, C. Park, Effect of sulfurization temperature on the efficiency of SnS solar cells fabricated by sulfurization of sputtered tin precursor layers using effusion cell evaporation, *J. Alloys Compd.* 806 (Oct. 2019) 410–417, <https://doi.org/10.1016/j.jallcom.2019.07.168>.
- [3] P. Sinsermsuksakul, et al., Overcoming efficiency Limitations of SnS-based solar cells, *Adv. Energy Mater.* 4 (15) (Oct. 2014) 1400496, <https://doi.org/10.1002/aenm.201400496>.
- [4] V. Steinmann, et al., 3.88% efficient tin sulfide solar cells using Congruent thermal evaporation, *Adv. Mater.* 26 (44) (Nov. 2014) 7488–7492, <https://doi.org/10.1002/adma.201402219>.
- [5] M. Minbashi, A. Ghobadi, M.H. Ehsani, H. Rezagholipour Dizaji, N. Memarian, Simulation of high efficiency SnS-based solar cells with SCAPS, *Sol. Energy* 176 (Dec. 2018) 520–525, <https://doi.org/10.1016/j.solener.2018.10.058>.
- [6] M. Taniguchi, R.L. Johnson, J. Ghijssen, M. Cardona, Core excitons and conduction-band structures in orthorhombic Ge,S, SnS, and SnSe single crystals, *Phys. Rev. B* 42 (6) (Aug. 1990) 3634–3643, <https://doi.org/10.1103/PhysRevB.42.3634>.
- [7] K.T. Ramakrishna Reddy, P. Purandar Reddy, R.W. Miles, P.K. Datta, Investigations on SnS films deposited by spray pyrolysis, *Opt. Mater.* 17 (1–2) (Jun. 2001) 295–298, [https://doi.org/10.1016/S0925-3467\(01\)00052-0](https://doi.org/10.1016/S0925-3467(01)00052-0).
- [8] T. Garmim, et al., Optical, electrical and electronic properties of SnS thin films deposited by sol gel spin coating technique for photovoltaic applications, *J. Mater. Sci. Mater. Electron.* 31 (23) (Dec. 2020) 20730–20741, <https://doi.org/10.1007/s10854-020-04586-y>.
- [9] S.H. Chaki, M.D. Chaudhary, M.P. Deshpande, SnS thin films deposited by chemical bath deposition, dip coating and SILAR techniques, *J. Semiconduct.* 37 (5) (May 2016) 053001, <https://doi.org/10.1088/1674-4926/37/5/053001>.
- [10] L. Zhao, et al., In situ growth of SnS absorbing layer by reactive sputtering for thin film solar cells, *RSC Adv.* 6 (5) (2016) 4108–4115, <https://doi.org/10.1039/C5RA2414H>.
- [11] R.W. Miles, O.E. Ogah, G. Zoppi, I. Forbes, Thermally evaporated thin films of SnS for application in solar cell devices, *Thin Solid Films* 517 (17) (Jul. 2009) 4702–4705, <https://doi.org/10.1016/j.tsf.2009.03.003>.
- [12] I.Y. Ahmet, et al., Evaluation of AA-CVD deposited phase pure polymorphs of SnS for thin films solar cells, *RSC Adv.* 9 (26) (2019) 14899–14909, <https://doi.org/10.1039/C9RA01938C>.
- [13] N.P. Klochko, et al., Development of a new thin film composition for SnS solar cell, *Sol. Energy* 134 (Sep. 2016) 156–164, <https://doi.org/10.1016/j.solener.2016.04.031>.
- [14] S. Gohri, J. Madan, R. Pandey, Enhancing the efficiency of SnS-based solar cells using a GLAD technique and CZTSSe layer, *Solid State Commun.* 377 (Jan. 2024) 115380, <https://doi.org/10.1016/j.ssc.2023.115380>.
- [15] S. Badyakar, C. Das, Numerical simulations on a-Si:H/SnS/ZnSe based solar cells, *Mater. Today Proc.* 62 (2022) 5275–5282, <https://doi.org/10.1016/j.matpr.2022.03.309>.
- [16] Md.S. Islam, N. Islam, Md. Anis-Uz-Zaman, A. Baul, S.M.G. Mostafa, M. Sreelekha, Investigation for optimal structure of CdS/SnS solar cell from numerical analysis, in: 2019 International Conference on Intelligent Sustainable Systems (ICISS), IEEE, Feb. 2019, pp. 447–450, <https://doi.org/10.1109/ISS1.2019.8908032>.
- [17] A. Kuddus, S.K. Mostaque, J. Hossain, Simulating the performance of a high-efficiency SnS-based dual-heterojunction thin film solar cell, *Opt. Mater. Express* 11 (11) (Nov. 2021) 3812–3826, <https://doi.org/10.1364/OME.439629>.
- [18] J. Xu, Y. Yang, Study on the performances of SnS heterojunctions by numerical analysis, *Energy Convers. Manag.* 78 (Feb. 2014) 260–265, <https://doi.org/10.1016/j.enconman.2013.10.062>.
- [19] S. Lin, et al., Numerical analysis of in Ga1–N/SnS and Al Ga1–N/SnS heterojunction solar cells, *Energy Convers. Manag.* 119 (Jul. 2016) 361–367, <https://doi.org/10.1016/j.enconman.2016.04.059>.
- [20] F. Jafarzadeh, H. Agihli, H. Nikbakht, S. Javadpour, Design and optimization of highly efficient perovskite/homojunction SnS tandem solar cells using SCAPS-1D, *Sol. Energy* 236 (Apr. 2022) 195–205, <https://doi.org/10.1016/j.solener.2022.01.046>.
- [21] K.G. Deepa, J. Nagaraju, Development of SnS quantum dot solar cells by SILAR method, *Mater. Sci. Semicond. Process.* 27 (Nov. 2014) 649–653, <https://doi.org/10.1016/j.mssp.2014.08.006>.
- [22] R. Garain, A. Basak, U.P. Singh, Study of thickness and temperature dependence on the performance of SnS based solar cell by SCAPS-1D, *Mater. Today Proc.* 39 (2021) 1833–1837, <https://doi.org/10.1016/j.matpr.2020.06.185>.
- [23] A.M.S. Arulanantham, S. Valanarasu, A. Kathalingam, M. Shkhir, H.-S. Kim, An investigation on SnS layers for solar cells fabrication with CdS, SnS₂ and ZnO window layers prepared by nebulizer spray method, *Appl. Phys. A* 124 (11) (2018) 776, <https://doi.org/10.1007/s00339-018-2164-6>.
- [24] S. Ahmed, A. Aktar, J. Hossain, A.B.M. Ismail, Enhancing the open circuit voltage of the SnS based heterojunction solar cell using NiO HTL, *Sol. Energy* 207 (2020) 693–702, <https://doi.org/10.1016/j.solener.2020.07.003>.
- [25] N.K. Reddy, Growth-temperature dependent physical properties of SnS Nanocrystalline thin films, *ECS Journal of Solid-State Science and Technology* 2 (6) (Apr. 2013) P259–P263, <https://doi.org/10.1149/2.006306jss>.
- [26] A. Hosen, S.R. Al Ahmed, Performance analysis of SnS solar cell with a hole transport layer based on experimentally extracted device parameters, *J. Alloys Compd.* 909 (Jul. 2022) 164823, <https://doi.org/10.1016/j.jallcom.2022.164823>.
- [27] N. Juneja, et al., Sb₂S₃ solar cells with a cost-effective and dopant-free fluorene-based enamine as a hole transport material, *Sustain. Energy Fuels* 6 (13) (2022) 3220–3229, <https://doi.org/10.1039/D2SE00356B>.
- [28] A. Basak, U.P. Singh, Numerical modelling and analysis of earth abundant Sb₂S₃ and Sb₂Se₃ based solar cells using SCAPS-1D, *Sol. Energy Mater. Sol. Cells* 230 (Sep. 2021) 111184, <https://doi.org/10.1016/j.solmat.2021.111184>.
- [29] U.A. Shah, S. Chen, G.M.G. Khalaf, Z. Jin, H. Song, Wide bandgap Sb₂S₃ solar cells, *Adv. Funct. Mater.* 31 (27) (Jul. 2021) 2100265, <https://doi.org/10.1002/adfm.202010265>.
- [30] S. Barthwal, R. Gupta, A. Kumar, K. Ramesh, S. Pathak, S. Karak, Band offset engineering in antimony sulfide (Sb₂S₃) solar cells, using SCAPS simulation: a route toward PCE > 10, *Optik (Stuttg)* 282 (2023) 170868, <https://doi.org/10.1016/j.ijleo.2023.170868>.
- [31] Y. Xiao, H. Wang, H. Kuang, Numerical simulation and performance optimization of Sb₂S₃ solar cell with a hole transport layer, *Opt. Mater. (Amst.)* 108 (2020) 110414, <https://doi.org/10.1016/j.optmat.2020.110414>.
- [32] S. Rahman, S.R. Al Ahmed, Photovoltaic performance enhancement in CdTe thin-film heterojunction solar cell with Sb₂S₃ as hole transport layer, *Sol. Energy* 230 (Dec. 2021) 605–617, <https://doi.org/10.1016/j.solener.2021.10.036>.
- [33] M.N.H. Riyad, A. Sunny, M.M. Khatun, S. Rahman, S.R. Al Ahmed, Performance evaluation of WS₂ as buffer and Sb₂S₃ as hole transport layer in CZTS solar cell by numerical simulation, *Eng. Reports* 5 (5) (May 2023) e12600, <https://doi.org/10.1002/eng.212600>.
- [34] S.R. Al Ahmed, A. Sunny, S. Rahman, Performance enhancement of Sb₂Se₃ solar cell using a back surface field layer: a numerical simulation approach, *Sol. Energy Mater. Sol. Cells* 221 (Jul. 2021) 110919, <https://doi.org/10.1016/j.solmat.2020.110919>.
- [35] G. Pan, et al., Substrate structured Sb₂S₃ thin film solar cells fabricated by rapid thermal evaporation method, *Sol. Energy* 182 (Apr. 2019) 64–71, <https://doi.org/10.1016/j.solener.2019.02.014>.
- [36] N.K. Reddy, M. Devika, K.R. Gunasekhar, E.S.R. Gopal, Fabrication of photovoltaic devices using ZnO nanostructures and SnS thin films, *Nano* 11 (7) (Jul. 2016) 1650077, <https://doi.org/10.1142/S1793292016500776>.
- [37] Z.G. Wang, W.C. Gao, J. Li, K.G. Liu, Development of SnS thin films for solar cells, *Appl. Mech. Mater.* 556–562 (May 2014) 278–281. <https://doi.org/10.4028/www.scientific.net/AMM.556-562.278>.
- [38] A. Benami, T. Ouslimane, L. Et-taya, A. Sohani, Comparison of the effects of ZnO and TiO₂ on the performance of perovskite solar cells via SCAPS-1D software package, *J. Nano-Electron. Phys.* 14 (1) (2022), [https://doi.org/10.21272/jnep.14\(1\).01033](https://doi.org/10.21272/jnep.14(1).01033).

- [39] Y. Raoui, H. Ez-Zahraouy, N. Tahiri, O. El Bounagui, S. Ahmad, S. Kazim, Performance analysis of MAPbI₃ based perovskite solar cells employing diverse charge selective contacts: simulation study, Sol. Energy 193 (Nov. 2019) 948–955, <https://doi.org/10.1016/j.solener.2019.10.009>.
- [40] A. Boubakri, A. Joudri, Y. Koumya, A. Rajira, A. Almagoussi, A. Abounadi, An output characteristics simulation of SnS based solar cells, Mater Today Proc 51 (2022) 2047–2052, <https://doi.org/10.1016/j.matpr.2021.07.428>.
- [41] M.W. Alam, et al., Preparation and characterization of Cu and Al doped ZnO thin films for solar cell applications, Crystals 12 (1–11) (Jan. 2022) 128, <https://doi.org/10.3390/cryst12010128>.
- [42] S.A. Ansari, et al., Directly grown of NiCo₂S₄ nanoparticles on a conducting substrate towards the high-performance counter electrode in dye-sensitized solar cell: a combined theoretical and experimental study, Sol. Energ. Mater. and Sol. Cells 225 (1–7) (March 2021), <https://doi.org/10.1016/j.solmat.2021.111064>.
- [43] S.A. Ansari, et al., “Solvothermal growth of 3D flower-like CoS@FTO as high-performance counter electrode for dye-sensitized solar cell, “, J. Mater. Sci. Mater. Electron. 30 (March 2019) 6929–6935, <https://doi.org/10.1007/s10854-019-01008-6>.
- [44] A. Haddout, A. Raidou, M. Fahoume, A review on the numerical modeling of CdS/CZTS-based solar cells, Appl. Phys. A 125 (2019) 1–16.
- [45] M. Djinkwi Wanda, S. Ouédraogo, F. Tchoffo, F. Zougmoré, J.M.B. Ndjaka, Numerical investigations and analysis of Cu₂ZnSnS₄ based solar cells by SCAPS-1D, Int. J. Photoenergy 2016 (2016).
- [46] H.T. Ganem, A.N. Saleh, Enhancement of the efficiency of the CZTS/CdS/ZnO/ITO solar cell by back reflection and buffer layers using SCAPS-1D, Iraqi J. Sci. (2021) 1144–1157.
- [47] M.A. Nalanya, et al., Numerical study of lead free CsSn_{0.5}Ge_{0.5}I₃ perovskite solar cell by SCAPS-1D, Optik (Stuttgart) 248 (Dec. 2021) 168060, <https://doi.org/10.1016/j.ijleo.2021.168060>.
- [48] S. Karthick, S. Velumani, J. Bouclé, Experimental and SCAPS simulated formamidinium perovskite solar cells: a comparison of device performance, Sol. Energy 205 (Jul. 2020) 349–357, <https://doi.org/10.1016/j.solener.2020.05.041>.
- [49] M. Burgelman, K. Decock, J. Verschraegen, A. Niemegeers, S. Degraeve, Simulation programme SCAPS-1D for thin film solar cells developed at ELIS, University of Gent, University of Gent, Dept. Electronics and Information Systems (ELIS) Pietersnieuwstraat 41 B-9000 Gent (Feb. 23, 2022). Belgium.
- [50] M. Burgelman, J. Verschraegen, S. Degraeve, P. Nollet, Modeling thin-film PV devices, Prog. Photovoltaics Res. Appl. 12 (23) (Mar. 2004) 143–153, <https://doi.org/10.1002/pip.524>.
- [51] M. Burgelman, P. Nollet, S. Degraeve, Modelling polycrystalline semiconductor solar cells, Thin Solid Films 361–362 (Feb. 2000) 527–532, [https://doi.org/10.1016/S0040-6090\(99\)00825-1](https://doi.org/10.1016/S0040-6090(99)00825-1).
- [52] J. Verschraegen, M. Burgelman, Numerical modeling of intra-band tunneling for heterojunction solar cells in SCAPS, Thin Solid Films 515 (15) (May 2007) 6276–6279, <https://doi.org/10.1016/j.tsf.2006.12.049>.
- [53] S. Degraeve, M. Burgelman, P. Nollet, Modelling of polycrystalline thin film solar cells: new features in SCAPS version 2.3, Proc. Of 3rd World Conf. on Photovolt. Energy Convers. 1 (2003) 487–490. ISBN:4-9901816-0-3.
- [54] M. Burgelman, J. Marlein, Analysis of graded band gap solar cells with SCAPS, Proc. Of the 23rd Eur. Photovolt. Sol. Energy Conf. (2008) 2151–2155. Valencia.
- [55] P.R. Michael, D.E. Johnston, W. Moreno, A conversion guide: solar irradiance and lux illuminance, Journal of Measurements in Engineering 8 (4) (Dec. 2020) 153–166, <https://doi.org/10.21595/jme.2020.21667>.
- [56] J. Greulich, H. Höffler, U. Würfel, S. Rein, Numerical power balance and free energy loss analysis for solar cells including optical, thermodynamic, and electrical aspects, J. Appl. Phys. 114 (20) (Nov. 2013) 204504, <https://doi.org/10.1063/1.4832777>.
- [57] M.G. Helander, M.T. Greiner, Z.B. Wang, W.M. Tang, Z.H. Lu, Work function of fluorine doped tin oxide, J. Vac. Sci. Technol. A: Vacuum, Surfaces, and Films 29 (1) (Jan. 2011), <https://doi.org/10.1116/1.3525641>.
- [58] Y. Zhou, et al., A universal method to produce low-work function electrodes for organic electronics, Science 336 (6079) (1979) 327–332, <https://doi.org/10.1126/science.1218829>. Apr. 2012.
- [59] J.O. Hwang, et al., Workfunction-tunable, N-doped reduced graphene transparent electrodes for high-performance polymer light-emitting diodes, ACS Nano 6 (1) (Jan. 2012) 159–167, <https://doi.org/10.1021/nn203176u>.
- [60] A. Cantas, et al., Importance of CdS buffer layer thickness on Cu₂ZnSnS₄ -based solar cell efficiency, J. Phys. D Appl. Phys. 51 (27) (Jul. 2018) 275501, <https://doi.org/10.1088/1361-6463/aac8d3>.
- [61] V. Stevanović, K. Hartman, R. Jaramillo, S. Ramanathan, T. Buonassisi, P. Graf, Variations of ionization potential and electron affinity as a function of surface orientation: the case of orthorhombic SnS, Appl. Phys. Lett. 104 (21) (May 2014), <https://doi.org/10.1063/1.4879558>.
- [62] S. Lyu, W.R.L. Lambrecht, Band alignment of III-N, ZnO and II-IV-N₂ semiconductors from the electron affinity rule, J. Phys. D Appl. Phys. 53 (1) (Jan. 2020) 015111, <https://doi.org/10.1088/1361-6463/ab4baa>.
- [63] B. Hussain, A. Aslam, T. Khan, M. Creighton, B. Zohuri, Electron affinity and bandgap optimization of zinc oxide for improved performance of ZnO/Si heterojunction solar cell using PC1D simulations, Electronics (Basel) 8 (2) (Feb. 2019) 238, <https://doi.org/10.3390/electronics8020238>.
- [64] A. Sahoo, I. Mohanty, S. Mangal, Effect of acceptor density, thickness and temperature on device performance for tin-based perovskite solar cell, Mater Today Proc (May 2022), <https://doi.org/10.1016/j.matpr.2022.05.095>.
- [65] M.T. Islam, A.K. Thakur, Two stage modelling of solar photovoltaic cells based on Sb₂S₃ absorber with three distinct buffer combinations, Sol. Energy 202 (May 2020) 304–315, <https://doi.org/10.1016/j.solener.2020.03.058>.
- [66] Y. Cao, et al., Towards high efficiency inverted Sb₂Se₃ thin film solar cells, Sol. Energy Mater. Sol. Cell. 200 (Jul. 2019) 109945, <https://doi.org/10.1016/j.solmat.2019.109945>.
- [67] X. Jin, et al., Solution processed NiO_x hole-transporting material for all-inorganic planar heterojunction Sb₂S₃ solar cells, Sol. Energy Mater. Sol. Cell. 185 (Oct. 2018) 542–548, <https://doi.org/10.1016/j.solmat.2018.06.017>.
- [68] S.A. Moiz, A.N.M. Alahmadi, M.S. Alshaikh, Lead-free FAcSnI₃ based perovskite solar cell: designing hole and electron transport layer, Nanomaterials 13 (9) (2023), <https://doi.org/10.3390/nano13091524>.
- [69] M.S. Salem, et al., Analysis of hybrid hetero-homo junction lead-free perovskite solar cells by SCAPS simulator, Energies 14 (18) (2021) 5741.
- [70] A. Bag, R. Radhakrishnan, R. Nekovei, R. Jeyakumar, Effect of absorber layer, hole transport layer thicknesses, and its doping density on the performance of perovskite solar cells by device simulation, Sol. Energy 196 (2020) 177–182, <https://doi.org/10.1016/j.solener.2019.12.014>.
- [71] S. Pyshkin, J. Ballato, Optoelectronics: Advanced Materials and Devices, BoD-Books on Demand, 2013.
- [72] S. Kant Sharma, Investigations on Nanocrystalline ZnO Thin Film Based Heterojunctions for Electronic and Photonic Device Applications Submitted by, 2016.
- [73] Matin, et al., Variation with Temperature, 2021. Ahmed et al., and 2021 khatun et al.
- [74] Bouich, et al., varshni, and 2012 sing et al., “short circuit current variation with temperature, 1967.
- [75] N. Kahoul, M. Houabes, M. Sadok, Assessing the early degradation of photovoltaic modules performance in the Saharan region, Energy Convers. Manag. 82 (Jun. 2014) 320–326, <https://doi.org/10.1016/j.enconman.2014.03.034>.
- [76] T. S. M. Sze Department of Electronics Engineering National Chiao Tung University Hsinchu and T. S. J. C. Kwok K. Ng Central Laboratory MVC (A Subsidiary of ProMOS Technologies, Physics Of Semiconductor Devices Third Edition.
- [77] MORALES-ACEVEDO A Publisher INTECH ISBN 9789535110033, Solar Cells Research and Application Perspectives Edition 2014 by MORALES-ACEVEDO A, INTECH.
- [78] B.E. Nieuwenhuys, Correlation between work function change and degree of electron back-donation in the adsorption of carbon monoxide and nitrogen on group VIII metals, Surf. Sci. 105 (2–3) (Apr. 1981) 505–516, [https://doi.org/10.1016/0039-6028\(81\)90015-7](https://doi.org/10.1016/0039-6028(81)90015-7).
- [79] B. Ofunye, J. Lee, M. Yan, C. Sun, J.-M. Zuo, I. Adesida, Electrical and microstructural properties of thermally annealed Ni/Au and Ni/Pt/Au Schottky contacts on AlGaN/GaN heterostructures, Semicond. Sci. Technol. 29 (9) (Sep. 2014) 095005, <https://doi.org/10.1088/0268-1242/29/9/095005>.
- [80] S. Trasatti, Work function, electronegativity, and electrochemical behaviour of metals, J. Electroanal. Chem. Interfacial Electrochem. 33 (2) (Dec. 1971) 351–378, [https://doi.org/10.1016/S0022-0728\(71\)80123-7](https://doi.org/10.1016/S0022-0728(71)80123-7).
- [81] A. Kumar, A.D. Thakur, Improvement of efficiency in CZTSSe solar cell by using back surface field, IOP Conf. Ser. Mater. Sci. Eng. 360 (Oct. 2018) 012027, <https://doi.org/10.1088/1757-899X/360/1/012027>.
- [82] O.K. Simya, A. Mahabobbatcha, K. Balachander, A comparative study on the performance of Kesterite based thin film solar cells using SCAPS simulation program, Superlattices Microstruct 82 (Jun. 2015) 248–261, <https://doi.org/10.1016/j.spmi.2015.02.020>.
- [83] V.E. González-Flores, R.N. Mohan, R. Ballinas-Morales, M.T.S. Nair, P.K. Nair, Thin film solar cells of chemically deposited SnS of cubic and orthorhombic structures, Thin Solid Films 672 (Feb. 2019) 62–65, <https://doi.org/10.1016/j.tsf.2018.12.044>.
- [84] J. Kang, S.-M. Kwon, S.H. Yang, J.-H. Cha, J.A. Bae, C.-W. Jeon, Control of the microstructure of SnS photovoltaic absorber using a seed layer and its impact on the solar cell performance, J. Alloys Compd. 711 (Jul. 2017) 294–299, <https://doi.org/10.1016/j.jallcom.2017.04.001>.
- [85] J.Y. Cho, S. Sinha, M.G. Gang, J. Heo, Controlled thickness of a chemical-bath-deposited CdS buffer layer for a SnS thin film solar cell with more than 3% efficiency, J. Alloys Compd. 796 (Aug. 2019) 160–166, <https://doi.org/10.1016/j.jallcom.2019.05.035>.
- [86] R.K. Yadav, P.S. Pawar, K.E. Neerugatti, R. Nandi, J.Y. Cho, J. Heo, Effect of intrinsic ZnO thickness on the performance of SnS/CdS-based thin-film solar cells, Curr. Appl. Phys. 31 (Nov. 2021) 232–238, <https://doi.org/10.1016/j.cap.2021.09.009>.
- [87] T.D. Nguyen, et al., Synthesis of Ag-embedded SnS films by the RF method for photovoltaic applications, Surface. Interfac. 25 (Aug. 2021) 101151, <https://doi.org/10.1016/j.surfin.2021.101151>.
- [88] M. Tamilselvan, et al., Planar heterojunction solar cell employing a single-source precursor solution-processed Sb₂S₃ thin film as the light absorber, ACS Omega 4 (2019) 11380–11387, <https://doi.org/10.1021/acsomega.9b01245>.
- [89] Chao Chen, Tang Jiang, Open-circuit voltage loss of antimony chalcogenide solar cells: status, origin and possible solution, ACS Energy Lett. 5 (7) (2020) 2294–2304, <https://doi.org/10.1021/acsenergylett.0c00940>.
- [90] A. Boubakri, A. Joudri, Y. Koumya, A. Rajira, A. Almagoussi, A. Abounadi, An output characteristics simulation of SnS based solar cells, Mater Today Proc 51 (2022) 2047–2052, <https://doi.org/10.1016/j.matpr.2021.07.428>.
- [91] H. Ullah, B. Mari, Numerical analysis of SnS based polycrystalline solar cells, Superlattices Microstruct 72 (Aug. 2014) 148–155, <https://doi.org/10.1016/j.j.physica.2014.03.042>.
- [92] Maykel Courel, Thalía Jiménez, A. Arce-Plaza, D. Seuret-Jiménez, J.P. Morán-Lázaro, F.J. Sánchez-Rodríguez, A theoretical study on Sb₂S₃ solar cells: the path to overcome the efficiency barrier of 8, Sol. Energy Mater. Sol. Cell., vol. 201 (2019) 110123, <https://doi.org/10.1016/j.solmat.2019.110123>.